Advances in Colloid and Interface Science 277 (2020) 102107

Contents lists available at ScienceDirect

Advances in Colloid and Interface Science

journal homepage: www.elsevier.com/locate/cis

Historical perspective

Ion partitioning and permeation in charged low-T^* membranes

Viatcheslav Freger [a,b,c,*]

[a] Wolfson Department of Chemical Engineering, Technion – IIT, Haifa 32000, Israel
[b] Russel Berrie Nanotechnology Institute, Technion – IIT, Haifa 32000, Israel
[c] Grand Technion Energy Program, Technion – IIT, Haifa 32000, Israel

ARTICLE INFO

Article history:
15 January 2020
Available online 20 January 2020

Keywords:
Ion-separating membranes
Ion transport in polymers
Ion association
Ion solvation
Ion mobility
Primitive model

ABSTRACT

Understanding ion transport in membrane materials is key to engineering and development of desalination and water purification technologies as well as electro-membrane applications. To date, modeling of ion transport has mainly relied on mean-field approaches, originally intended for weak inter-ionic interactions, i.e., high reduced temperature T^*. This condition is violated in many membranes, which could explain disagreement between predicted trends and experiments. The paper highlights observed discrepancies and develops a new approach based on the concept of ion association, more adequate in the low-T^* limit. The new model addresses ion binding and mobility consistently within the same physical picture, applied to different types of single and mixed salts. The resulting relations show a significantly weaker connection between ion partitioning and permeability than the standard ones. Estimates using primitive model (PM) of ions in a homogeneous dielectric suggest that non-PM mechanisms, originating from the molecular structure of the ion-solvating environment, might enhance ion association in membranes. PM analysis also predicts that ion solvation and association must be rigidly related, yet non-PM effects may decouple these phenomena and allow a crossover to non-trivial regimes consistent with experiments and simulations. Despite the crude nature of the presented approach and some questions remaining open, it appears to explain most available experimental data and presents a step towards predictive modeling of ion-selective membrane separations in water-, environment- and energy-related applications.

Contents

Abbreviations: DH, Debye-Hückel; HTT, hindered-transport theory; MSD, mean-square displacement; PB, Poisson-Boltzmann; PM, primitive model; RPM, restricted primitive model; SDE, Steric-Donnan-deElectric model.

* Corresponding author at: Wolfson Department of Chemical Engineering, Technion – IIT, Haifa 32000, Israel.
E-mail address: vfreger@technion.ac.il.

https://doi.org/10.1016/j.cis.2020.102107
0001-8686/

1. Introduction

Today reverse osmosis (RO) and nanofiltration (NF) are mature technologies widely utilized to desalinate and purify water from natural reservoirs as well as wastewater to millions of people worldwide [1,2]. Its core element is the polymeric thin-film composite membranes that pass water yet reject ions. RO usually removes all ions to a high degree, while NF is similar and uses essentially the same type of membranes but may separate different ions as well as ions and non-ionic components.

Ion selectivity in RO has not been a major concern in process engineering, however, NF requires models that can predict ion separation for ion mixtures that may widely differ in salinity and ion composition. Development of such models is intimately related to understanding the physics underlying different rejection of specific ions. Unfortunately, the currently used models still leave many questions open and do not offer a treatment fully consistent with observations [3,4]. The main purpose of this paper is to highlight and address the major gaps and inconsistencies of the currently used physical models of NF and RO. Another purpose is to propose reasonably simple picture that may help to improve the current models and move closer to predictive modeling.

The presently used models commonly rely on so-called mean-field relations [5], such as the Poisson-Boltzmann (PB) equation or simpler Donnan and related models, to compute averaged potentials and concentrations [6,7]. In the present context, such relations pertain to a regime where the reduced temperature T^* is high, i.e., the relevant interaction energy is always small on the thermal k_BT scale. We will see, however, that such an assumption is inconsistent with typical physical characteristics of most RO, NF, as well as many ion-conducting membranes. As a result, effects not amenable to mean-field treatment and thus missing in the current models, most notably, *ion association* [8], become important and may profoundly change the physical picture.

In this paper, we develop a more appropriate type of models using the approach pioneered by Bjerrum for ionic solutions [9]. The resulting general relations are reasonably simple but suit better the low-T^* regimes. This is shown to yield trends that, in contrast to current models, may explain the experimental data. As a further insight, we also compute relevant parameters of the model, affinities and association constants, based on representative physical characteristics of the membrane and ions, using the *primitive model* (PM), i.e., treating the membrane phase as a homogeneous dielectric continuum and ions, mobile or fixed, as hard spheres [10]. This highlights limitations of using PM and emphasize the need to address complex mechanisms that go beyond simple PM electrostatics, which will have to be clarified in the future.

The paper is organized as follows. Sections 2 and 3 review the standard phenomenological equations of ion transport relations and treatment of ion exclusion in homogeneous membranes along mean-field lines and highlight the major inconsistencies. Section 4 reviews the main relations for ion association. Section 5 develops the new general approach to modeling ion partitioning and permeation. Section 6 analyzes the model relations based on PM and highlights discrepancies between its predictions and experimental results. Finally, Sections 7 outlines extension of the approach to multi-salt mixtures and Section 8 presents summary and outlook, including the relation of the present treatment to the ion transport in nanopores.

2. Ion permeation in NF and RO: general relations and representative results

2.1. Basic phenomenological relations: extended Nernst-Planck equation

The general basis of most currently used models of RO and NF is the extended Nernst-Planck (ENP) equation that describes steady-state transport of an ionic species through a membrane [11]. For a *homogeneous* membrane of uniform thickness, the problem is reduced to one-dimensional. For practical calculation, when membrane thickness is uncertain, it is convenient to convert intrinsic permeability to permeance and scale the normal coordinate x by the membrane thickness Δx, i.e., define $\bar{x} = x/\Delta x$, thus the ENP equation for ion i is written as follows [12].

$$\begin{aligned} J_i &= -P_i C_i\left(\frac{d\mu_i}{dx} + z_i\frac{d\varphi}{dx}\right) + J_V(1-\sigma_i)C_i \\ &= -\omega_i C_i\left(\frac{d\mu_i}{d\bar{x}} + z_i\frac{d\varphi}{d\bar{x}}\right) + J_V(1-\sigma_i)C_i. \end{aligned} \tag{1}$$

where J_i and z_i are flux and charge of ionic species i, μ_i is the dimensionless chemical potential if i (in units of thermal energy k_BT), φ the dimensionless electric potential (in units of thermal potential k_BT/e), J_V the volume flux, and ω_i, P_i, and σ_i are, respectively ion permeance (often called permeability), intrinsic (thickness-normalized) permeability, and reflection coefficient.[1]

When the membrane is viewed as a homogeneous "black box", ω_i and σ_i are phenomenological coefficients, relating ion fluxes to so-called virtual or corresponding concentration of the ion C_i. The latter are defined as the hypothetical solution concentrations that would be in equilibrium with the state of the membrane at the specific location x. For an

[1] For consistency with the subsequent sections, concentrations and activities are expressed as the number of solute particles (ions) per unit volume and thermodynamic quantities (energies, chemical potentials etc.) are per solute particle, unless specified otherwise. The corresponding molar concentrations, fluxes, and energies are obtained by dividing the number quantities by the Avogadro number $N_A = 6 \times 10^{23}$ 1/mol.

ideal solution, the virtual concentration will be identical to ion activity ($C_i = a_i$), thereby chemical potential is $\mu_i = \ln a_i = \ln C_i$.[2] For real solutions, virtual concentrations C_i offer a simple and transparent way to gauge the local thermodynamic state within the membrane in terms of equilibrium solution composition that continuously vary across membrane-solution interfaces. Note that non-ideality in solution is nearly always much smaller than within the membrane. The use of C_i in place of a_i, i.e., assuming $\mu_i \approx \ln C_i$, is then a reasonable approximation that marginally affects the accuracy of modeling and will be used throughout this paper.

We may express ion fluxes in Eq. (1) through permeate concentrations $C_i'' = J_i/J_V$, i.e., the value of C_i at the downstream side of the membrane. Eq. (1) then becomes

$$C_i'' = -\frac{\omega_i C_i}{J_V}\left(\frac{d\mu_i}{d\bar{x}} + z_i\frac{d\varphi}{d\bar{x}}\right) + (1-\sigma_i)C_i \approx -\frac{\omega_i}{J_V}\left(\frac{dC_i}{d\bar{x}} + z_i C_i\frac{d\varphi}{d\bar{x}}\right) + (1-\sigma_i)C_i. \tag{2}$$

The "black box" of ω_i and σ_i may be opened to some degree by relating the actual local concentration in the membrane c_i to virtual concentration C_i through the local partitioning (sorption) coefficients $S_i = c_i/C_i$. In addition, the ion mobilities and coupling of ion fluxes J_i to pressure-driven water flow J_V may be expressed through ion diffusivities (mobilities) D_i or, alternatively, friction coefficients $f_i = k_BT/D_i$. Since there are at least 3 kinds of species involved, namely, membrane (m), solvent (water, w) and ions (i), full phenomenological description of ion transport in presence of moving water requires at least two friction coefficients, namely, ion-membrane f_{im} and ion-water f_{iw}.. Ultimately, this yields the phenomenological relations for P_i, ω_i and σ_i [12]:

$$\omega_i = \frac{D_i S_i}{\Delta x} = \frac{1}{\Delta x}\frac{k_BTS_i}{f_{im}+f_{iw}}, P_i = \omega_i\Delta x = D_iS_i = \frac{k_BTS_i}{f_{im}+f_{iw}},$$
$$1-\sigma_i = \frac{S_i}{\phi_w}\frac{f_{iw}}{f_{im}+f_{iw}}, \tag{3}$$

where ϕ_w is the volume fraction of water in the membrane. Note that both diffusive (ω_i) and convective (1-σ_i) coefficients are proportional to S_i. Since partitioning is in general concentration- and composition-dependent, so are the coefficients ω_i and σ_i. However, S_i and its concentration dependence are cancelled out in the so-called Péclet coefficients, defined as follows [12].

$$A_i = \frac{1-\sigma_i}{\omega_i} = \frac{f_{iw}\Delta x}{k_BT\phi_w}. \tag{4}$$

A_i is then a purely frictional parameter; for this reason, it could replace either ω_i or σ_i for analysis of frictional characteristics, such as effective pore size of the membranes. The product $Pe_i = AJ_V$ is the well-known membrane Péclet number that indicates which contribution to the ion transport, convective ($Pe \gg 1$) or diffusive ($Pe \ll 1$), is dominant. Note that, unlike A_i, Pe_i is not a constant and depends on J_V, which varies with the applied pressure.

Since A and Pe are proportional to the membrane thickness Δx (Eq. (4)), for a very thin membrane $AJ_V \ll 1$ may hold in all reasonable situations [13,14]. This is apparently the case for ion permeation in today's composite NF and RO membranes, in which

$\Delta x << 1$ μm and the usable fluxes J_V are limited by concentration polarization (CP), i.e., mass transfer in the adjacent unstirred solution layer. In such a case, Eqs. (1) and (2) may be simplified to have only the diffusion term on the r.h.s.

Note, the condition $AJ_V \ll 1$ alone is insufficient to simply drop the convective term in Eqs. (1) or (2). In general, elimination of the convective term also requires that ω_i be replaced with a composite parameter ω_i/σ_i, thereby σ_i is not totally eliminated from the equation. However, if in addition to $AJ_V \ll 1$, the membrane is selective enough, thereby $\sigma_i \approx 1$, the reflection coefficient disappears entirely from Eqs. (1) and (2) [14]. Both conditions are well satisfied for ionic solutes in today's NF and RO membranes, in which case only ω_i's are required for predicting separation performance [6,13,14]. The resulting equation is fully analogous to the regular NP equation for ion transport in solutions [15], except that ion diffusivities are replaced with permeabilities ω_i or P_i, i.e., to a good approximation,

$$C_i'' \approx -\frac{P_i}{J_V}\left(\frac{dC_i}{dx} + z_iC_i\frac{d\varphi}{dx}\right) = -\frac{\omega_i}{J_V}\left(\frac{dC_i}{d\bar{x}} + z_iC_i\frac{d\varphi}{d\bar{x}}\right). \tag{5}$$

Steady-state transport for a solution of N ionic species through a membrane is modeled by linking a set of such ENP (Eq. (2)) or, approximately, NP equations (Eq. (5)) for individual ions to two conditions of electroneutrality (charge stoichiometry), one for local composition and one for ionic fluxes, as follows

$$X + \sum_{i=1}^{N} z_ic_i = X + \sum_{i=1}^{N} z_iS_iC_i = 0, \tag{6a}$$

$$J_V\sum_{i=1}^{N} z_iC_i'' = I/e. \tag{6b}$$

Here X is the fixed (immobile) charge density of the membrane and I is the electric current density, which is zero, unless a non-zero current is imposed on the system by applying an external potential gradient. Given the feed composition $\mathbf{C}'$ (a vector containing concentrations of all ions) and dependence of coefficients ω_i and σ_i on virtual solution composition ($\mathbf{C}$), the full set of NP or ENP equation (Eqs. (2) or (5)) subject to electroneutrality (Eqs. (6)) is solved for a given J_V to yield $\mathbf{C}''$ and ion fluxes $\mathbf{J} = J_V\mathbf{C}''$. In general, this requires numerical integration, which usually starts from guessing the permeate composition $\mathbf{C}''$ followed by iterative integration of Eqs. (2) or (5) backward from permeate ($\mathbf{C}''$) to feed side ($\mathbf{C}'$) and correction of $\mathbf{C}''$ until compositions converge. (Note that the iterative forward integration from feed to permeate is often unstable.)

In some important cases, the ENP equations may be solved analytically. One such case is the feed containing a single salt $M_{z-}A_{z+}$ of a cation M^{z+} and an anion A^{-z-} of absolute charges z_+ and z_-. The respective virtual ion concentrations are related to that of the salt C_s as $C_+ = z_-C_s$ and $C_- = z_+C_s$. For zero current, the potential gradient is eliminated to yield a single equation for salt transport

$$C_s'' = \frac{C_-''}{z_+} = \frac{C_+''}{z_-} = -\frac{\omega_s}{J_V}\frac{dC_s}{d\bar{x}} + (1-\sigma_s)C_s. \tag{7}$$

Eq. (7) is identical to the well-known Spiegler-Kedem (SK) equation for transport of neutral solutes [16], in which the "salt" chemical potential μ_s and coefficients ω_s and σ_s and are related to ionic counterparts as follows

$$\mu_s = z_+\mu_- + z_-\mu_+ = z_+\ln(z_+C_s) + z_-\ln(z_-C_s), \tag{8}$$

$$\omega_s = \frac{\omega_+\omega_-(z_+ + z_-)}{\omega_+z_+ + \omega_-z_-}, \quad \sigma_s = \sigma_- - \frac{\omega_+z_+}{\omega_+z_+ + \omega_-z_-} + \sigma_+\frac{\omega_-z_-}{\omega_+z_+ + \omega_-z_-}. \tag{9}$$

For constant ω_s and σ_s, a well-known analytical solution of the SK equation, Eq. (7), is

$$\frac{C_s''}{C_s'} = \frac{1-\sigma_s}{1-\sigma_s\exp(-Pe_s)}, \tag{10}$$

[2] The constant chemical potential of the reference state is dropped here as inessential, since it cancels out in all subsequent relations.

where $Pe_s = J_V(1\text{-}\sigma_s)/\omega_s$. This solution predicts a monotonic increase of solute passage C_s''/C_s' with J_V, with an initial slope ω_s/σ_s at small Pe_s and approach to a plateau value $1\text{-}\sigma_s$ at large Pe_s.

An analytical solution may also be obtained, though with more effort, for mixtures of one dominant salt with dilute trace ions [17,18]. In this situation, the trace ions have a negligible effect on the electric potential profile $\varphi(x)$ that is fully determined by the dominant salt. The passage of the dominant salt is then computed in the same manner as for a single salt (Eq. (7)), while for trace ions Eq. (2) is solved for fixed $\varphi(x)$. The solution for trace ions may lead to non-linear and non-monotonic dependence on J_V, much different from Eq. (10). This feature allows evaluation of ionic permeabilities from filtration data, despite the fact that the problem is ill-posed in general (see next). This solution was also found useful for analyzing practical problems, such as pH variations in desalination, which results from transport of protons H^+ or hydroxyls OH^-, behaving as trace ions, superimposed on transport of dominant NaCl salt [19].

2.2. Ionic and salt permeabilities from filtration data: experimental results

Modeling NF using an appropriate set of ENP or NP equations requires knowledge of phenomenological coefficients for all ions. Even when the reflection coefficients are redundant (Eq. (5)), this still requires all ion permeabilities as input parameters. Unfortunately, they cannot be adequately predicted at present and, therefore, need to be assessed from filtration experiments by fitting them to the NP model as adjustable parameters.

In general, such a fitting is an ill-posed problem, since ion fluxes are coupled by electroneutrality (Eqs. (6)). This coupling eliminates one degrees of freedom and, as a result, ionic permeabilities cannot be uniquely determined. For instance, for a single salt, cation and anion must permeate at the same rate to keep electroneutrality. The measurable parameter is then only the salt permeability, ω_s, defined in Eq. (9), but individual values of ω_+ and ω_- may assume virtually any values, as long as they yield the same ω_s.

Similarly, in a ternary mixture, e.g., of NaCl and $CaCl_2$, the total anion flux carried by chloride has to match exactly the total cationic flux made up by Na^+ and Ca^{2+}. This is highlighted in Fig. 1, mapping the fitting error obtained when Ca^{2+} permeability was fitted to ternary permeation data for NF270 membrane, while Na^+ and Cl^- permeabilities were prescribed fixed values [4]. The valley colored in dark blue designates various combinations of Na^+ and Cl^- permeabilities, for which the fitting error has a minimal and virtually the same magnitude. However, the uncertainty becomes much smaller, if one considers salt permeabilities of NaCl and $CaCl_2$, defined as follows (cf. Eq. (9))

$$\omega_{NaCl} = \frac{2\omega_{Na}\omega_{Cl}}{\omega_{Na}+\omega_{Cl}},\ \omega_{CaCl_2} = \frac{3\omega_{Ca}\omega_{Cl}}{2\omega_{Ca}+\omega_{Cl}}. \tag{11}$$

Along the valley, all combinations of Na^+ and Cl^- permeabilities yield about the same fitted values of ω_{NaCl} and ω_{CaCl2}, therefore the two salt permeabilities are determined with a much larger certainty than individual ion permeabilities.

Thus deduced salt permeabilities would be insufficient for NF modeling. Yet, their values and observed dependence on concentration (for single salts) or on total composition (for mixtures) may be useful for comparing with theoretical predictions and serve as fingerprints of specific physical models. Such comparison may help gain valuable insights and discriminate or rule out possible mechanisms, as discussed next.

2.3. NF: representative results and trends for single salts and mixtures

Fig. 2A presents typical dependences deduced from NF filtration data for several single salts [3]. A few points are immediately notable. First, salt permeability varies with the feed salt concentration, while the variation may be both increasing and decreasing, depending on the salt type. Increasing trends are observed for salts of monovalent cations (Na^+, K^+), yet for salts of divalent cations (Ca^{2+}, Mg^{2+}) a *decreasing* trends is observed, as reported in other studies as well [13,20]. Note the valence of anion seems to have no effect on the trend, though it may strongly affects the values of permeability (cf. NaCl versus Na_2SO_4). The decreasing trends of Ca^{2+} and Mg^{2+} salts contradict the

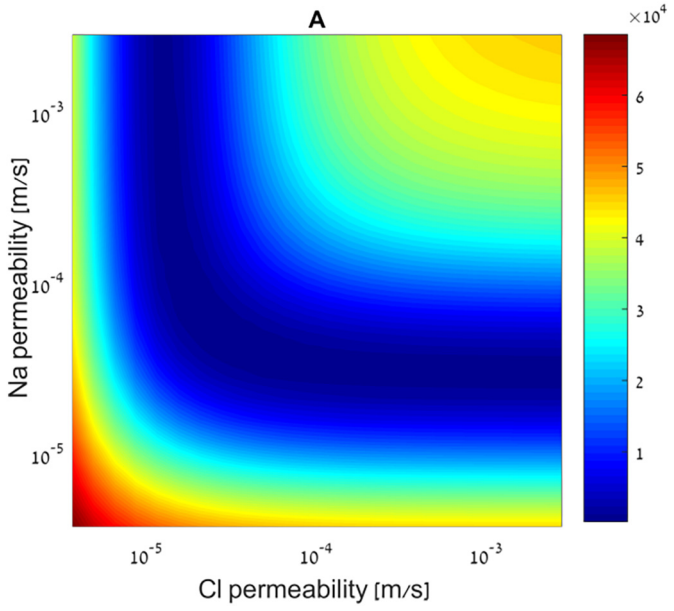

Fig. 1. The error map produced by fitting the Ca^{2+} permeability to NF filtration data for NaCl and $CaCl_2$ mixtures for prescribed values of Na^+ and Cl^- permeabilities shown on vertical and horizontal axes, respectively. Membrane NF270, all solutions contain 0.1 M total chloride. After reference [4].

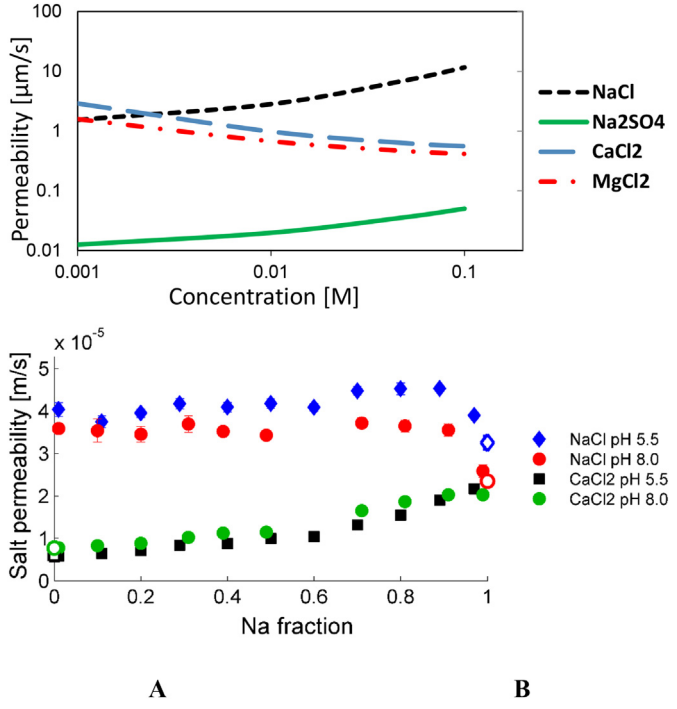

Fig. 2. (A) Variation of salt permeability with salt concentration estimated from filtration data for single salts and NF200 membrane [3]; (B) Variation of NaCl and $CaCl_2$ permeabilities through NF270 membranes for NaCl/$CaCl_2$ mixtures at two different pH for different Na fraction in the feed. All mixtures contain 0.1 M total chloride. Permeabilities are deduced by fitting the NP model with constant ion permeabilities to the filtration data [4].

standard mean-field relations (see next section), which predict that a single salt permeability must always increase with concentration. Moreover, even for more "regularly" behaving permeabilities of NaCl in Fig. 2A, the slope is smaller than the theoretical value 1. It also becomes smaller at low salt concentrations, which is opposite of what the mean-field models anticipate.

Fig. 2B highlights further discrepancies inconsistent with common models. It displays fitted permeabilities of NaCl and $CaCl_2$ in for mixed feed solutions, of total 0.1 M chloride but different ratios of Ca^{2+} and Na^+, at two different pH [4]. A lower pH (more H^+) must always suppresses permeation of cations and promotes that of anions. This is supposed to increase salt permeability, since one expects that salt permeation in a negatively charged membrane would be controlled by anions. Indeed, in the present case, NaCl permeability is higher at lower pH, i.e., Cl^- is the less permeable ion in NaCl, however, for $CaCl_2$ it is opposite, indicating that Cl^- is the more permeable ion in $CaCl_2$.

The results in Fig. 2B further indicate that Ca^{2+} and Na^+ affect each other's permeability in a manner resembling competitive binding or adsorption on some sites. Such sites might well be the negative fixed charges of NF-270, as they should bind divalent Ca^{2+} more strongly than monovalent Na^+. Indeed, addition of a small fraction of Ca^{2+} seems to have an immediate effect on NaCl permeation, which quickly plateaus as more Ca^{2+} is added. Similarly, addition of Na^+ increases $CaCl_2$ permeability, yet in a more moderate monotonic manner across the entire composition range. Unfortunately, the concept of ion binding or association is absent in the common models of NF and is incompatible with their mean-field nature. A notable exception is the model by Bandini and Mazzoni that added specific ion binding in ad hoc manner [21].

These and other observations mentioned later on point to fundamental flaws in the current picture of ion exclusion and permeation. To see that systematically, the following sections briefly review commonly used mean-field relations. Their defining feature is that the varying potential imposed by the fixed charges within the membrane is replaced with some *average or weakly varying smeared effective potential, known as Donnan potential* [22]. We will show that such replacement results in inherent inconsistencies, which is the main reason for their failure. Thereafter, in Section 5 we will outline an approach that can eliminate such inconsitencies, in line with up-to-date views on electrolyte solutions [8,10], and apply it to analyzing ion transport in membranes.

3. Ion permeation through a homogeneous membrane: mean-field relations

3.1. Permeability: partitioning and diffusivity factors

Based on Eq. (3), computation of ion permeabilities P_i required for NF modeling usually involves independent assessment of diffusivities D_i and partitioning coefficients Γ_i. The simplest approach, dominating in membrane literature, employs two major approximations [7,23–37].

(1) Each mobile ion is assigned a single value of diffusivity or, equivalently, mobility throughout the membrane phase;
(2) The potential within the membrane phase is approximated with a uniform or slowly varying "mean-field" potential profile, also known as Donnan potential, whose value ensures the membrane phase electroneutrality (Eq. (6a)).

In a uniform force or concentration gradient fields, diffusivity of an ion reflects its friction with the medium, which may be evaluated using various approaches. Most common has been the hindered transport theory (HTT) that assumes rigid pores of fixed uniform size and a rigid solute particle [38]. Apart from the questionable extension of continuum hydrodynamics to ions in nanopores, another shortcoming is that this dictates a sharp drop in mobility when the solute size approaches the pore size, while experiments show a more moderate variation. As a remedy, it was proposed to consider a distribution of pore sizes, at the expense of a larger number of parameters [39–41]. An alternative approach to modeling diffusivity in membanes, uncommon in NF or RO but common in gas separation, is to consider elastic or dynamic pores that may undergo thermal fluctuations around an equilibrium size and occasionally pass solutes larger than this size [42,43]. Nevertheless, within all these approaches, the diffusivities D_i are viewed as a frictional property, unrelated or weakly related to thermodynamics and contributing only a constant prefactor to P_i. This means that most of the concentration dependence must be related to *ion partitioning* S_i, reviewed next. However, we return to the diffusivities in Section 5, for the case when the mean-field no more applies.

3.2. Partitioning in a charged homogeneous membrane: Donnan and SDE models

The simplest model of ion partitioning, widely employed in the membrane literature, is the Donnan model that considers a homogeneous membrane that bears a fixed charge of a uniform density X [22]. For concreteness, we assume X is negative thus anions and cations are, respectively, co- and counter-ions.

In the classical Donnan model, the sole role of the fixed charge is to break the stoichiometry between counter- and co-ions. Apart from that, ions in the membrane phase behave ideally with activity coefficient $\gamma_i = a_i/c_i = 1$. Setting $\varphi = 0$ for the external solution, broken stoichiometry in the membrane is equivalent to imposing a Donnan potential $\varphi = \varphi_D$ on the entire membrane phase. This potential uniformly raises the concentration of counter-ions and reduces that of co-ions, resulting in an overall exclusion of invading salt.

The classical Donnan model ignores ion-specific effects other than ion charge (valence). To introduce ion specificity, the next-level approximations include ionic activity coefficients γ_i that may incorporate non-idealities, such as steric constraints and solvation. *Ion solvation* reflects the *dielectric properties*, i.e., medium *polarizability*, which increases the enthalpy of a single ion in a low-dielectric membrane compared with high-dielectric aqueous solution [44–46]. *Steric exclusion* similarly increases γ_i, but its origin is *entropic*; reflecting restrictions on translation, rotation and vibration of ions confined in pores [42]. These effects raise ion's *excess partial free energy* in the membrane g_i^E. If expressed in k_BT units, it is related to the activity coefficient as follows

$$\gamma_i = \exp(g_i^E). \tag{12}$$

Following Yaroshchuk [47], it may be more intuitive to use a non-Donnan partitioning coefficient or *affinity* k_i instead of γ_i. When the solution phase is assumed nearly ideal ($g_{i,\,sol}^E \approx 0$, $\gamma_{i,\,sol} \approx 1$), k_i and γ_i are related as

$$k_i = \frac{\gamma_{i,sol}}{\gamma_i} = \exp\left[-\left(g_i^E - g_{i,sol}^E\right)\right] \approx \frac{1}{\gamma_i} = \exp(-g_i^E). \tag{13}$$

Given k's or all ions, the ion partitioning is found by requiring equal *electrochemical potential* of each ion ψ_i in the solution and membrane phases. The (dimensionless) electrochemical potential is defined as

$$\psi_i = \mu_i \pm z_i\varphi, \tag{14}$$

where the sign corresponds to the ion charge.

Since φ is unknown a priori, it might be easier to define and solve equilibrium relations for *independent salts* rather than ions. For example, in a mixture of Na^+, Ca^{2+}, and Cl^-, such independent salts will be NaCl and $CaCl_2$. Since salts are neutral, electric potential cancels out and the chemical and electrochemical potentials of a salt become identical. For a binary salt $M_{z-}A_{z+}$ one then obtains

$$\begin{aligned}\mu_s &= z_+\mu_- + z_-\mu_+ = z_+ \ln C_- + z_- \ln C_+ \\ &= z_+ \ln(c_-/k_-) + z_- \ln(c_+/k_+)\end{aligned} \tag{15}$$

or

$$c_-^{z_+} c_+^{z_-} = (k_- C_-)^{z_+} (k_+ C_+)^{z_-}. \quad (16)$$

For a single salt in a charged membrane, the electroneutrality further dictates that $c_- = z_+ c_s$ and $c_+ = z_- c_s + X/z_+$, where c_s is the concentration of the *invading free salt*, thereby

$$c_s^{z_+} (c_s + X/z_- z_+)^{z_-} = (k_- C_s)^{z_+} (k_+ C_s)^{z_-}, \quad (17)$$

Solving Eq. (17) yields the relation between c_s and C_s and free-salt partitioning coefficient $S_s = c_s/C_s$.

An alternative procedure is through explicit use of the Donnan potential φ_D, which is cancelled out in Eq. (16) but appears in the relations for individual ions, i.e.,

$$c_i = k_i C_i \exp(-z_i \varphi_D). \quad (18)$$

Combining such relations for all ions with electroneutrality, yields φ_D and c_s.

It is straightforward to generalize the solution to any number of ions and salts by writing down and solving either Eq. (17) for all independent neutral salts or Eq. (18) for all ions along with electroneutrality (Eq. (6)). Solving the resulting set of non-linear equations will yield both φ_D and partitioning $S_i = c_i/C_i$ of each ion. Note that analytical solution for mixed salts may not be possible in general. One important case amenable to analytical solution is a mixture of a dominant salt with dilute trace ions [17–19].

3.3. The excess free energy and ion affinities: PM relations

Practically, the affinities $k_i = \gamma_{i,\,sol}/\gamma_i \approx 1/\gamma_i$ may be treated as adjustable parameters, but there is much interest to compute them using appropriate physical relations. The commonly used one that combines steric exclusion and solvation is

$$k_i = \Phi_i \exp(-\Delta W_i), \quad (19)$$

where Φ_i is the (entropic) Ferry steric exclusion factor and ΔW_i is the difference in the dimensionless (in k_BT units) self-energy W_i, the solvation energy of an ion, between the membrane and solution phases.

The solvation energy W_i is often approximated using the Born equation, based on PM, i.e., the view of ions as charged solid spheres in a dielectric continuum [10,48]. When inter-ion interactions are ignored, the dimensionless Born self-energy of an ion is

$$W_i = \frac{z_i^2 e^2}{8\pi\varepsilon_0 \varepsilon r_i k_B T} = z_i^2 \frac{\lambda_B}{2 r_i}, \quad (20)$$

where r_i is the ion radius, ε the dielectric constant (relative permittivity), and λ_B is the Bjerrum length of the membrane phase defined as the distance between monovalent ions, at which the electrostatic interaction energy equals k_BT. λ_B is essentially a characteristic of the membrane only, given by

$$\lambda_B = \frac{e^2}{4\pi\varepsilon_0 \varepsilon k_B T}. \quad (21)$$

Eqs. (12)–(20) define a mean-field model of ion exclusion, hereafter referred to as the Steric-Donnan-diElectric (SDE) model [3]. It is the generic basis of many transport models of NF and RO, as well as in electro-membrane processes, such as electrodialysis, membrane electrolysis, and fuel cells [49].

3.4. SDE model: the neutral and charged membrane regimes

Real membranes often contain fixed charges, however, if their content is small, the membrane may behave essentially as a neutral one that bears no fixed charge. The distinction between charged and neutral membranes depends on how the fixed charge density X compares with the concentration of the invading salt c_s. Eq. (17) gives the general solution; however, it is expedient to consider two limiting regimes. For clarity, we limit the analysis to the case of a single salt.

The "neutral" regime is obtained when $c_s >> X$. In this case, Eq. (17) predicts a constant salt partitioning coefficient S_s [3].

$$S_s \equiv \frac{c_s}{C_s} \approx S_0 = k_+^{\frac{z_-}{z_+ + z_-}} k_-^{\frac{z_+}{z_+ + z_-}}. \quad (22)$$

We will refer to the parameter S_0, defined by Eq. (22), as *salt injection coefficient* that determines overall affinity of the membrane to salt and will be used extensively below. For instance, the condition of a "neutral" membrane $c_s >> X$ is redefined for the solution concentration as $C_s >> X/S_0$.

Another limiting regime of a "charged" membrane, also known as "good co-ion exclusion" [11,33], is obtained in the opposite case when the fixed charge largely exceeds the invading salt, i.e., $c_s << X$ or $C_s << X/S_0$. Eq. (17) then predicts a concentration-dependent salt partitioning [3].

$$S_s \approx k_- \left[k_+ z_+ z_- \frac{C_s}{X} \right]^{z_-/z_+}. \quad (23)$$

Eq. (17), as well as Eqs. (22) and (23), indicate that S_s should either stay constant or increase with C_s, but *may never decrease*. Since the salt permeability ω_s is proportional to S_s (cf. Eq. (2)), the same must hold for salt permeability. Unfortunately, ω_s often exhibits a C_s dependence that contradicts this and other conclusions, as highlighted in Section 2.3. There are also a few other inconsistencies, such as large discrepancies between fitted and independently measured physical characteristics of the membrane, most notably, X and ε [50–55].

We argue that the actual reason is the *mean-field* nature of SDE model that ignores the local variations of the inter-ionic potential and thus greatly underestimates the ion-ion interaction energy. As explained below, mean field fails when this energy is large. Since both W_i and ion-ion interactions are governed by essentially the same physical parameters, i.e., ion sizes and membrane dielectric constant, a situation in which both W_i is large and local potential variations are small is impossible. The SDE model is then *fundamentally flawed* in charged low-dielectric membranes, which includes most membranes used in RO, NF and many electro-membrane separations.

4. When the mean-field breaks down: ion association

4.1. Characteristic length scales analysis

The concept of a uniform Donnan potential implies that, if overall electroneutrality is satisfied, the entropy or thermal energy k_BT dominates over all inter-ionic interactions and smears potential variations. Whether this condition is satisfied may be directly tested by comparing relevant length scales [56,57]. One natural length scale is set by the Bjerrum length λ_B, a membrane characteristic (Eq. (21)). The dimensionless Coulomb energy $U(x)$ of interaction between two ions i and j is the ratio of λ_B or, for multivalent ions, $z_i z_j \lambda_B$, to the ion-ion distance x

$$U(x) = \frac{z_i z_j \lambda_B}{x} \cong \frac{\lambda_B}{x}. \quad (24)$$

The distance x has natural lower and upper bounds. The former is the distance of closest approach $b = r_i + r_j$, where r_i and r_j are the ionic radii. The upper bound L is determined by the average inter-ion spacing, approximately equal to $c^{-1/3}$, where c is the characteristic ion

concentration in the membrane. The natural choice is $c = c_s = S_0 C_s$ for a neutral membrane and $c = X$ for a charged one.

Another often used length scale is the Debye screening length λ_D, which is the distance, below which an ion significantly perturbs the surrounding ionic "atmosphere" [58]. However, this length is not independent and related to L and λ_B [56]. Indeed, after inserting the ion, the change in entropy of the atmosphere would just balance the change in electrostatic energy. The unperturbed atmosphere of radius λ_D contains on average $N_0 = \lambda_D^3/L^3$ ions, which increases to $N_0 + 1$ after inserting the central ion thus entropy changes by $\Delta s = \ln[(N_0+1)/N_0] = \ln(1 + L^3/\lambda_D^3) \approx L^3/\lambda_D^3$ (in k_B units). The corresponding gain in electrostatic energy in k_BT units is (up to a numerical factor) λ_B/λ_D, since the atmosphere's charge is on average λ_D away from the central ion. Equating the two yields λ_D, as follows.

$$\Delta s \approx L^3/\lambda_D^3 \cong \lambda_B/\lambda_D \text{ or } \lambda_D^2 \cong L^3/\lambda_B. \tag{25}$$

Note this analysis and the very notion of λ_D are only meaningful when the atmosphere contains many ions, i.e., $L^3/\lambda_D^3 << 1$ [58], which means $\lambda_D >> L$ or, equivalently, $\lambda_B << L$.

We see that the three length scales b, L and λ_B fully define the system and set the maximal and minimal values of electrostatic energy relative to the thermal energy. Three cases are possible:

1. When $\lambda_B \sim b << L$, the thermal energy dominates over electrostatics and effectively "stirs" the system so that majority of ions dissociate. This is the typical situation in water, as well as strongly hydrated membranes or hydrogels, where $\lambda_B = 0.7$ nm is commensurate with the diameters of most inorganic ions (0.2–0.7 nm) and is much smaller than L (at least a few nm for $C_s \sim 1$ M). The concept of smeared Donnan potential is then applicable. Dissociated ions behave as nearly free species, but there still may be some weak collective effects addressed by the Debye-Hückel (DH) theory.
2. In another extreme, $\lambda_B > L$, the ions are spaced so closely that the thermal energy becomes weaker than ion-ion electrostatic interactions. Majority of ions should associate, forming ion pairs, triplets etc., and only very few ions will be able to move freely. In these regime, mean-field-type models (SDE, PB etc.), as well as the DH theory and the very notions of Debye length and Donnan potential, will break down entirely. For instance, Eq. (25) indicates that in this regime $\lambda_D << L$, i.e., the Debye "atmosphere" occupies a volume unphysically smaller than the average volume per ion, i.e., will contains less than one ion. Such regime will require a non-mean-field treatment.
3. Between the above regimes, i.e., within the range $b < \lambda_B < L$, the situation may be viewed as coexistence of two states, free and associated. Approximate self-consistent theories for this case, also called "chemical models" [10], were first advanced by Bjerrum for ion solutions [9] and later by Katchalsky et al. [59] and Manning [60] for polyelectrolytes.

It is expedient to redefine cases 2 and 3 for a strongly charged membrane in terms of membrane characteristics. In a charge membrane, $L \approx X^{-1/3}$ and the condition $\lambda_B > L$ may be expressed as

$$\varepsilon < \frac{e^2}{4\pi\varepsilon_0 k_B T} X^{1/3}. \tag{26}$$

For typical fixed charge densities in ion-selective and desalination membranes, $X \sim 0.5$ M, case 2 will occur when $\varepsilon < 20$–30. Except for highly swollen hydrogels, most membrane materials [37], even containing a few 10% of water, should have average ε in this range. Mobile ions in such membranes will be subject to a strong non-uniform potential of fixed charges, which cannot be adequately replaced with a smeared Donnan potential. As an illustration, Fig. 3 shows the time-averaged ion concentration obtained in MD simulations of membrane-NaCl solution equilibrium [61]. It is seen that, except for largest water-filled cavities, Na^+ and Cl^- ions in a polyamide matrix tend to become localized around fixed charges, which bears little resemblance to the smeared Donnan-like distribution.

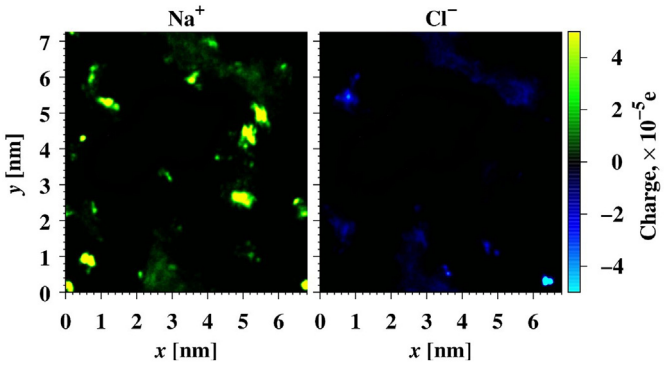

Fig. 3. Maps of Na^+ and Cl^- concentration in a polyamide membrane, presented as time-averaged ion charge per pixel, obtained in MD simulation of a polyamide network exposed to a NaCl solution. After reference [61].

A crucial observation is that for $\lambda_B > b$ (case 3) or more so for $\lambda_B > L >> b$ (case 2), the thermal energy will be small compared not only with the inter-ionic electrostatic energy, but with the Born solvation energy as well, as easily seen by comparing Eqs. (20) and (24). This means that the SDE model, simply combining the Born energy *and* a uniform Donnan potential, becomes *physically inconsistent and exceedingly poor* for many NF, RO and ion-selective membranes, most of which are both charged and low-dielectric. A correct model must address the fact that the actual potential around fixed charges within such membranes will be highly non-uniform, promoting a strong ion association in the form of pairs, triplets etc. The "chemical-model" approach, originated by Bjerrum, that self-consistently treats ion association is briefly reviewed in the next section.

4.2. Ion association in pairs, triplets and larger associates

Bjerrum considered the probability $dp(x)$ of finding two ions, a central one of charge z_+ and a closest "satellite" of charge z_-, at a distance between x and $x + dx$ in the following form [10,48].

$$\frac{dp(x)}{dx} = \frac{4\pi x^2 \langle e^{-U(x)} \rangle}{\int_b^L 4\pi x^2 \langle e^{-U(x)} \rangle dx} \approx \frac{x^2 \exp\left(\frac{z_+ z_- \lambda_B}{x}\right)}{\int_b^L x^2 \exp\left(\frac{z_+ z_- \lambda_B}{x}\right) dx}. \tag{27}$$

The exponent in Eq. (27) is the Boltzmann factor containing the dimensionless (in k_BT units) electrostatic energy of the satellite ion $U(x)$ averaged over the spherical shell $4\pi x^2 dx$. The denominator in Eq. (27) is the partition function or phase integral of a satellite ion over the average volume L^3 per ion ($L >> b$).

In dilute solutions, the probability of finding more than one satellite sufficiently close to the central ion is small and interaction with the other ions (multi-body interactions) may be ignored thus the potential may be approximated by the spherically symmetric Coulomb potential $U(x) \approx -z_+ z_- \lambda_B/x$. It is easy to see that for point-like charges, i.e., $b = 0$, the phase integral diverges, which means the solution will collapse to point-like neutral associates. Bjerrum pointed out that a finite b is crucial for preventing the association collapse [5].

The numerator in Eq. (27) has a minimum at $q = z_+ z_- \lambda_B/2$. On this basis, Bjerrum proposed to divide the total phase space $b \le x \le L$ to the "free" ($x > q$) and "associated" ($x < q$) states. He treated associates as neutral species and applied the DH theory to the free ions only. The distinction between associated and free species in the Bjerrum theory seems somewhat arbitrary, yet Bjerrum's choice of q was found to be

reasonable in most cases [62]. It was also shown that contribution of ion pairs to the electrostatic energy (ion-dipole interactions), ignored by Bjerrum, cannot be ignored for concentrated systems, close to the condensation transition of free ion "gas" to a dense ionic "liquid" [57]. Yet, Bjerrum's approach may reasonably describe the present case of dilute free ions.

The treatment is easiest for a symmetric 1:1 electrolyte forming neutral pairs. In this case $z_+ = z_- = 1$ and $q = \lambda_B/2$. In water $q \ll L$ (dilute solutions), the free-ion part of the phase integral ($q < x < L$) covers most of the solution volume, in which $\langle e^{-U(x)/kT}\rangle \approx 1$. This part is then roughly the average volume per cation or anion $L^3 = 1/c_+ = 1/c_-$. Using the Coulomb potential for computing the phase integral over the associated state ($b < x < q$) yields the association constant, analogous to association constants of weak electrolytes, as follows

$$K_2 = \frac{c_2}{c_+c_-} \approx 4\pi\int_b^q \left\langle e^{-U(x)}\right\rangle x^2dx \approx 4\pi\int_b^{\lambda_B/2} e^{\lambda_B/x}x^2dx$$
$$= Q_2\cdot 4\pi b^3\frac{b}{\lambda_B}e^{\lambda_B/b} \quad (28)$$

where c_2 is the concentration of pairs.

Eq. (28) is made more compact by defining the reduced temperature $T^* = b/\lambda_B$, as the thermal energy k_BT scaled by the electrostatic energy of the ion pair at tight contact ("ground state") [57,62]. Eq. (28) then becomes

$$K_2 = Q_2(b,T^*)\cdot 4\pi b^3T^*e^{1/T*} \approx 10^1b^3T^*e^{1/T*}. \quad (29)$$

The factor Q_2 approaches 1 when $T^* \ll 1$, which corresponds to the low-temperature ground state, and reaches a maximum of 3.36 at $T^* = 0.176$. The ground-state expression may then be a reasonable approximation, even if T^* is not very small. Eq. (29) can be generalized to symmetric (neutral) or asymmetric (charged) pairs of ions with charges z_+ and z_- in a dilute solution, in which case λ_B is simply multiplied by z_+z_- (Eq. (21)) and T^* is divided by the same factor.

The association constants for triplets, quadruplets etc. may be obtained by generalizing Bjerrum's analysis for pairs. Agua et al. derived the association constant for triplets composed of a central ion of absolute charge z and two satellite counter-ions of unit charge [62]. The result can be similarly presented as a product of the ground-state expression and a correcting term Q_3 that approaches 1 for $T^* \ll 1$, as follows

$$K_3 = Q_3\frac{32\pi^2}{(z-1/4)^2}b^6\left(\frac{b}{\lambda_B}\right)^3\exp\left[\frac{2z-1/2}{\lambda_B/b}\right] \approx 10^2b^6T^{*3}\exp\left[\frac{\alpha_3}{T^*}\right]. \quad (30)$$

The structure of expressions for pairs and triplets, Eqs. (29) and (30), may be understood as follows. The exponential factors of the form exp. (α/T^*), with $\alpha_2 = z$ for pairs or $\alpha_3 = 2z - ½ \cong 1$ for triplets, reflects the gain in the electrostatic energy (enthalpy) for the ground-state arrangement (Fig. 4). Conversely, the prefactors $V_2 \cong 10b^3T^*$ or $V_3 \cong 10^2b^6T^{*3}/V_2 \cong 10b^3T^{*2}$ may be understood as volumes, within which the second and third ions may still undergo residual thermal motion, relative to the other ions in the associate. The volumes determine the entropy loss upon association, $\Delta s_2 = -k_B\ln(c_sV_2)$, $\Delta s_3 = -k_B\ln(c_sV_3)$. For the second ion, this volume is a thin spherical shell of area $4\pi b^2$ and thickness $bT^* \ll b$ (dark-shaded region in Fig. 4A). For the third ion, this volume (dark-shaded region in Fig. 4B) is asymmetric and still smaller ~ b^3T^{*2}. For $T^* \ll 1$, the volumes V_2 and V_3 are much smaller than the volume of the ion pair (~b^3), that is, the ions are strongly immobilized, but reduced entropy is compensated by the gain in electrostatic energy.

It is uncommon to consider still larger multiplets, since the concentration of n-plets is proportional to C_s^n and should fall off rapidly below the salt solubility. However, the derivation can be generalized to larger multiplets [62]. The association constant of an n-plet will differ from its predecessor $(n-1)$-plet by a factor

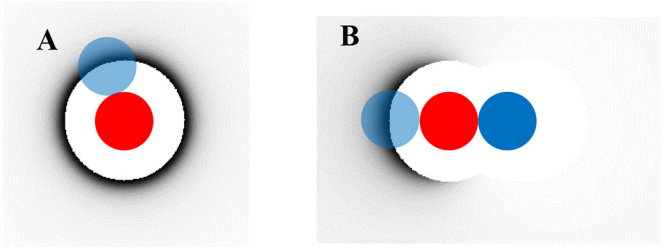

Fig. 4. Schematic maps of probability density of finding the center of a second and a third ions (shown in light blue), respectively, in a pair (A) and a triplet (B) composed of hard-sphere ions of the same diameter in a dielectric continuum. Darker grey shade corresponds to larger probability. The first ion in pair and triplet is shown in red and second ion in triplet in dark blue; their position is assumed to be fixed in ground-state arrangement relative to the last-added ion.

$$\theta_n = K_n/K_{n-1} = V_n\exp(\Delta\alpha_n/T^*), \quad (31)$$

where $0 < \Delta\alpha_n = \alpha_n - \alpha_{n-1} < 1$ and V_n~$10b^3T^{*m}$ with $1 \le m \le 2$ for monovalent ions of equal size. The analysis presented in Appendix shows that V_n and $\Delta\alpha_n$ hence θ_n vary fairly slowly with n and may be roughly seen as constants. We may then crudely view the association constants of increasingly large associates as a geometric series, where each subsequent term differs from its predecessor by a similar factor. This approximation will be used below.

5. Ion partitioning and association in a low-T^* membrane: general relations

5.1. Phase behavior of ionic fluids: general PM behavior

General features of ion fluid thermodynamics have been established using PM; most commonly the restrictive primitive model (RPM), in which all ions are of the same size and absolute charge. Fisher et al. summarized phase diagrams in reduced variables T^* and b^3c obtained for RPM by several analytical theoretical models and Monte Carlo (MC) simulations [57,62]. They showed that different models lead to fairly similar temperature-density phase diagrams, qualitatively resembling gas-liquid equilibria of regular fluids, with critical temperature $T^*_{cr} \approx 0.05 - 0.1$ and critical ion concentration $c_{cr}b^3 \approx 0.05 - 0.1$.

The region $T^* >> T^*_{cr}$ in the phase diagram represents situations far from formation of a dense condensed phase. In this regime, ions approach ideal solution-like behavior, when the Donnan model may well apply. Some weak corrections of mean-field type, such as the DH theory, or account for moderate Manning condensation, may improve accuracy [37,63,64]. Unfortunately, the deviations are expected to become exceedingly strong in NF, RO and many other ion-containing membranes, which are not excessively swollen and for which T^* ~ 0.05 to 0.2 is typical. We then focus here on this T^* range, for which ion association comes strongly into play.

It is expedient to stress the distinction between computing phase diagrams and ion partitioning in a membrane. The former has the ion concentration predetermined, which may be arbitrarily large and result in condensed states. In contrast, for the latter it is the activity or *virtual* concentration in the external phase that is fixed and determines the actual ion concentration in the membrane. Since affinity of low-T^* membrane phase to ions is small, a *non-charged (neutral) membrane* should take up only a small concentration of free ions, which would associate negligibly and are unlikely to form a condensed state (see next section).

However, if a membrane contains a large fixed charge of density X, it will impose ion concentrations otherwise non-attainable in the membrane phase in the low-T^* regime. Such excessive ion concentrations must promote ion "condensation" or association on fixed sites at ion activities that would not produce condensation in a neutral medium. (In a sense, this is

analogous to water uptake from unsaturated vapor by a hydrophilic sorbent.) This may greatly enhance *ion uptake* by a charge membrane.

However, in the context of *ion permeation*, a large uptake promoted by fixed charges may not be translated to proportionally larger permeability, since ions in free and asscotiated states of ions may significantly differ in effective mobility. This complicates the relation between ion-partitioning S_i and permeability ω_i (Eq. (3)). A treatment that consistently addresses both uptake and mobility of associated species within the same physical picture will be developed below.

5.2. Non-charged membrane: PM analysis

Consider first a membrane with a negligible charge $X \approx 0$. In the low-temperature regime $T^* << 1$ the association constants are large, however, the ion self-energy W_i is also large. This is immediately seen by re-writing the Born equation (Eq. (20)) in terms of T^*,

$$W_i = \frac{z_i^2 \lambda_B}{2r_i} = \frac{z_i^2 b}{2r_i} \frac{1}{T^*} \cong \frac{1}{T^*} >> 1. \tag{32}$$

Since W_i is large, salt injection coefficient S_0 is small and so is the free salt concentration in the membrane c_s. This is supposed to make concentration of n-plet associates, proportional to c_s^n, small as well. Association should then insignificantly affect salt permeation.

For example, let us use PM and consider a salt, not necessarily symmetric, made of a cation of charge z_+ and anion of charge z_- of equal radii $r_+ = r_- = b/2$ and ignore non-ideality in external solution phase and steric exclusion. Combining Eqs. (19), (20), and (22), the salt injection coefficient is obtained as

$$S_0 = \exp\left(-\frac{z_+ z_-}{T^*}\right). \tag{33}$$

The concentration of free salt and ions in the membrane is then

$$c_s = S_0 C_s, \quad c_+ = z_- c_s = z_- S_0 C_s, \quad c_- = z_+ c_s = z_+ S_0 C_s, \tag{34}$$

and the concentration of ion pairs c_2 (Eq. (28))

$$c_2 = K_2 c_+ c_- \cong b^3 \frac{T^*}{z_+ z_-} \exp\left(\frac{z_+ z_-}{T^*}\right) \times z_+ z_- C_s^2 \exp\left(-\frac{2 z_+ z_-}{T^*}\right) = b^3 C_s^2 T^* \exp\left(-\frac{z_+ z_-}{T^*}\right). \tag{35}$$

The associated ion fraction is then

$$\frac{c_2}{c_s} \cong b^3 C_s T^*. \tag{36}$$

This fraction must be small, since T^* is small and $b^3 C_s$ is the volume fraction of ions in solution, usually small as well (for instance, $b^3 C_s \approx 0.1$ for saturated ~6 M NaCl solution.). The ions pairs are then supposed to contribute negligibly to salt partitioning and permeation, as was concluded long ago in the context of lipid membranes [45,65].

As another way to confirm negligible association within PM, we may also verify that the distance $q = z_+ z_- \lambda_B/2 = z_+ z_- b/2T^*$ separating free and associated states is much smaller than the average distance between free ions in the membrane $L = c_s^{-1/3}$. Indeed, from Eq. (34), the ratio

$$\frac{q}{L} = b c_s^{1/3} \frac{z_+ z_-}{2T^*} \approx b C_s^{1/3} \frac{z_+ z_-}{2T^*} \exp\left(-\frac{z_+ z_-}{3T^*}\right) \tag{37}$$

must be small, since $b c_s^{1/3} = (b^3 c_s)^{1/3}$ is small (see above), whereas $\frac{z_+ z_-}{2T^*} \exp(-\frac{z_+ z_-}{3T^*})$ may never exceed $1.5/e \approx 0.55$ (maximum at $T^* = z_+ z_-/3$) and is small as well for $T^* << 1$. We conclude that, within PM, mean-field approximation may work reasonably well in neutral low-T^* (i.e., low-dielectric) membranes.

Nevertheless, PM may not always represent the real situation and this conclusion should be taken with caution. Even in water, certain salts are known to associate more strongly than PM predicts [8,10]. In a low-dielectric membrane, where electrostatics is enhanced and complicated by microheterogeneities and other effects, both S_0 and association constants are likely to deviate from PM (see Section 6.4). As a result, formation and permeation of pairs or even larger associates may become non-negligible. The consequences of non-PM behavior may become even more dramatic for charged membranes. For this reason, in the rest of this section, focused on charged membranes, we will first develop general relations and thereafter re-analyze them using PM in Section 6.

5.3. General equilibrium relations for a charged membrane

As already emphasized in Section 5.1, substantial fraction of fixed ionizable groups in a charged low-T^* membrane is expected to form associates with mobile ions. Consider first a membrane of fixed charge density X in equilibrium with solution of an MA salt, such as NaCl. Let us subdivide the membrane to unit near-spherical cells, each containing a fixed charge, spaced on average by a distance $L = (6\times/\pi)^{-1/3} \approx X^{-1/3}$, as schematically shown in Fig. 5. The cells may either remain empty, i.e., contain only the dissociated fixed charges X^- or contain mobile anions and/or cations as well. Since the cell radius $L/2$ is typically commensurate with or smaller than the distance $q = \lambda_B/2$, in the spirit of Bjerrum's theory we may refer to different non-empty states of a cell as neutral XM pairs, charged triplets XM_2^+ and XMA^- etc.

Since for small T^* the interaction with the fixed charge within a cell dominates over interactions with ions outside the cell, we may approximately consider each cell as independent and sum up the different states of a cell in a one-site grand partition function, as follows [58].

$$\xi = 1 + K_{XM}[M^+] + K_{XM_2}[M^+]^2 + K_{XMA}[M^+][A^-] + \ldots \tag{38}$$

where K's are appropriate binding constants that are essentially one-cell phase integrals (partition functions) for the corresponding states. $[M^+]$ and $[A^-]$ are the hypothetical concentrations that would be obtained in the membrane phase, subject to ion self-energy and electroneutrality but far from (i.e., not interacting with) any fixed charge. They play the role of electrochemical activities of the ions in the membrane or *free-ion concentrations*, if the membrane had room for free ions. Roughly, these concentrations should be measured at the boundaries (dashed lines) between the cells occupied by neutral XM pairs depicted as solid green circles in Fig. 5A. At these boundaries, the average potential directly imposed on the free ions by the fixed and mobile ions in the neighboring cells is presumably small, yet some residual Donnan-like background potential is possible, similar to a neutral membrane. Equilibrium with external solution requires that (cf. Eq. (16))

$$[M^+][A^-] = (S_0 C_s)^2, \tag{39}$$

where $S_0 = (k_M k_A)^{1/2}$ is the salt injection coefficient (cf. Eq. (33)).

The K's in Eq. (38) are similar to respective association constants (Section 4.2), except that the integration is over the entire cell volume, i.e., the upper limit is the cell radius $x = L/2$ rather than $x = q$. However, for small T^* the difference is negligible, since the integral is dominated by small distances $x \sim b << L$.

As a further approximation, restrict the summation in Eq. (38) to the states ("associates") with charges −1, 0 and + 1, since more charged states should be too few due to large uncompensated self-energy and/or the need to associate too many mobile ions (cf. c_s^n dependence of concentration of n-plets). These three groups of associates will form three "homologous" series formed by adding neutral pairs M^+A^- to either X^-, XM^0 or XM_2^+. The K constants for any such "homologue" may be represented as the product of the association constant of the predecessor homologue and a factorθ_{MA}, for instance, $K_{XM_2A} = \theta_{MA} K_{XM}$ (see Eq. (31)). By arguments of Eq. (30), the factors $\theta_{MA} = \theta_M \theta_A$ may

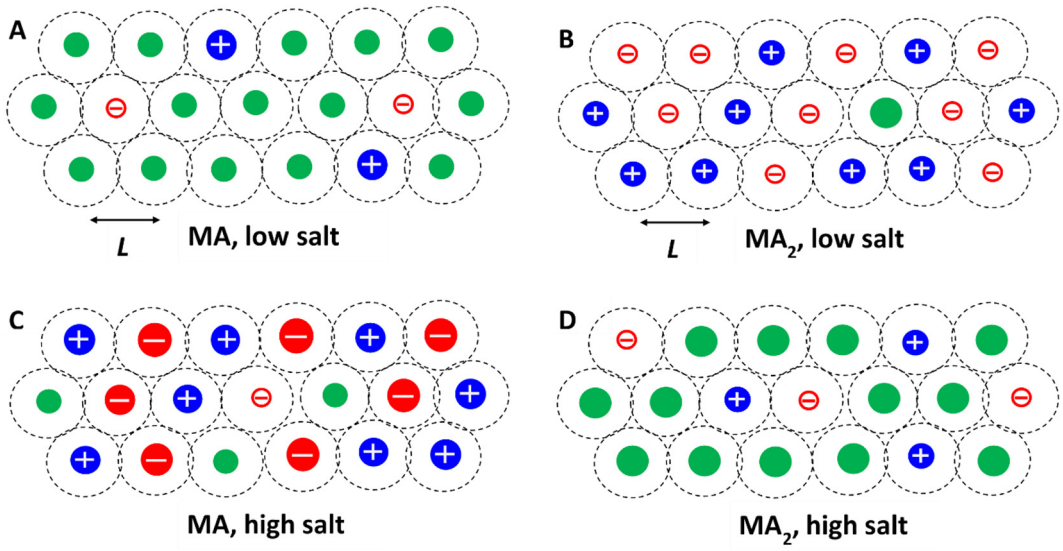

Fig. 5. Schematic snapshots of a charged membrane in equilibrium with solutions of an MA (A, C) or MA_2 (B, D) salt. Panels A and B are for low salt and C and D for high salt concentrations. Dashed line-encircled regions are unit cells, spaced at distance L, each containing a fixed charge. Small empty circles are dissociated fixed charges, medium-sized circles are XM pairs and largest circles are XM_2 or XMA triplets. Negative species are solid red with a minus sign, positive species are solid blue with a plus sign, and neutral ones are solid green. In panel A, a minor fraction of XMA^- triplets is not shown for simplicity.

somewhat vary between the three series and individual homologues but all are likely to be commensurate. Therefore, the term contributed to Eq. (38) by each homologue will differ from its predecessor in the series, e.g., XM_2A versus XM, by a factor

$$\Theta = \theta_{MA}[M^+][A^-] = \theta_{MA}S_0^2C_s^2 \cong \left(C_s b^3\right)^2 T^{*3} \exp\left(\frac{\Delta\alpha_M + \Delta\alpha_A - 2}{T^*}\right). \quad (40)$$

Based on PM relations, Eqs. (20), (29) and (31), and Eq. (16), the last expression is expected to be small, since $C_s b^3$, T^{*3} and the exponential factor must all be small (note $\Delta\alpha < 1$, cf. Eq. (31)). This means we might truncate Eq. (38) to just three first three terms (first homologues in each series). However, such truncation would leave no cells that contain A^- ions, which would be unphysical. Therefore, we keep in ξ the four terms shown in Eq. (38), which we now use as an approximation.

The average number of cations and anions per cell, expressed as the function of K's and S_0 and solution concentration C_s, may then obtained from ξ using the standard relation of statistical thermodynamics along with overall electroneutrality and Eq. (39). First, the electroneutrality dictates that the average charge per cell must be zero, i.e., $-1 + K_{XM_2}[M^+]^2 - K_{XMA}[M^+][A^-] = 0$ therefore (Eq. (39))

$$[M^+]^2 = \frac{1 + K_{XMA}(S_0C_s)^2}{K_{XM_2}}. \quad (41)$$

The average number of M^+ and A^- ions per cell is then

$$\overline{n}_M = [M^+]\frac{\partial \ln\xi}{\partial[M^+]} \approx \frac{K_{XM}[M^+] + 2K_{XM_2}[M^+]^2 + K_{XMA}[M^+][A^-]}{\xi} \approx 1 + \frac{K_{XMA}(S_0C_s)^2}{\xi}, \quad (42a)$$

$$\overline{n}_A = \overline{n}_M - 1 \approx \frac{K_{XMA}(S_0C_s)^2}{\xi}, \quad (42b)$$

where

$$\xi \approx K_{XM}\left(\frac{1 + K_{XMA}(S_0C_s)^2}{K_{XM_2}}\right)^{1/2} + 2\left[1 + K_{XMA}(S_0C_s)^2\right]. \quad (42c)$$

Eq. (42) are the key result of the present model that describes ion partitioning in the case of MA salts. Relations for an MA_2 salt of a divalent cation M^{2+} and a monovalent anion A^-, such as $CaCl_2$, are obtained similarly. The primary states of charge −1, +1 and 0 will be charged cells X^- and XM^+ and a neutral triplet XMA^0. Their homologues will be formed by adding neutral MA_2 combinations to primary states, but such large associates will be rare and again ignored here. The analogues of Eq. (38) and (39) will then be

$$\xi \approx 1 + K_{XM}\left[M^{2+}\right] + K_{XMA}\left[M^{2+}\right][A^-] \quad (43)$$

$$\left[M^{2+}\right][A^-]^2 = 4(S_0C_s)^3, \quad (44)$$

where $S_0 = (k_M k_A^2)^{1/3}$. Electroneutrality further requires that $-1 + K_{XM}[M^{2+}] = 0$, then

$$\left[M^{2+}\right] = 1/K_{XM}. \quad (45)$$

The average number of ions per cell will then be (note double charge of M^{2+} in Eq. (46b))

$$\overline{n}_M = \left[M^{2+}\right]\frac{\partial \ln\xi}{\partial\left[M^{2+}\right]} \approx \frac{K_{XM}\left[M^{2+}\right] + K_{XMA}\left[M^{2+}\right][A^-]}{\xi} \approx 1 - \frac{1}{\xi}, \quad (46a)$$

$$\overline{n}_A = 2\overline{n}_M - 1 \approx 1 - \frac{2}{\xi}, \quad (46b)$$

where

$$\xi \approx 2\left[1 + K_{XMA}\left(\frac{S_0^3C_s^3}{K_{XM}}\right)^{1/2}\right]. \quad (46c)$$

Eqs. (42) and (46) define adsorption isotherms of mobile ions on the fixed charges as a function of C_s. Since the overall concentration of ion i in the membrane is $c_i = \overline{n}_i X$, the *overall* ion partitioning coefficients for MA salts are.

$$S_A = \frac{\overline{n}_A X}{C_s} = \frac{X}{C_s}\frac{K_{XMA}(S_0C_s)^2}{\xi}; S_M \approx \frac{\overline{n}_M X}{C_s} = \frac{X}{C_s}\left[1 + \frac{K_{XMA}(S_0C_s)^2}{\xi}\right], \quad (47)$$

with ξ given by Eq. (42c). The corresponding expressions for MA_2 salts are

$$S_A = \frac{\overline{n}_A X}{2C_s} = \frac{X}{C_s}\left(\frac{1}{2} - \frac{1}{\xi}\right); S_M = \frac{\overline{n}_M X}{C_s} = \frac{X}{C_s}\left(1 - \frac{1}{\xi}\right), \quad (48)$$

with ξ given by Eq. (46c).

The above relations may be used to analyze ion partitioning data, such as ion exchange followed by spectroscopies such as ICP, RBS, XPS, scintillation, and UV–vis, or micro-weighing, that count overall ion content in the membrane [50,51,66–69]. However, Eqs. (47) and (48) *may not* be combined in Eq. (3) with the free ion mobilities D_A and D_M to compute permeabilities. The reason is that the mobile ions cease to behave as free ones when they bind to the fixed charges [63,70,71]. The appropriate general relations for mobilities and permeabilities will be developed in the next section.

It is expedient to highlight the trends predicted by Eqs. (47) and (48) in more detail. First, Eqs. (42c) and (46c) show that for dilute solutions (low salt), i.e., small C_s, ξ will approach a constant, $\xi \approx 2 + K_{XM}(K_{XM_2})^{-1/2}$ for MA salts and $\xi \approx 2$ for MA_2 salts. The resulting situation is schematically depicted in Fig. 5A and B, respectively. Remarkably, it is distinctly different for the two salt types, as MA will convert most of the fixed charges to neutral XM pairs (Fig. 5A), while MA_2 will result in about equal amounts of dissociated fixed charges X^- and oppositely charged XM^+ pairs (Fig. 5B). In either case, the membrane will contain very few triplets and co-ions, but the number of counter-ions per fixed charge will then approach 1 for M^+ and ½ for M^{2+} cations (cf. Eqs. (42a) and (46a)). This is in excellent agreement with RBS data by Coronell et al., who reported that, after wash of excess salt at different pH (which alters X), uptakes of Ag^+ and Ba^{2+} ions by the selective layer of RO membranes show a ratio very close to 2:1 for all pH values [67]. Obviously, this agreement may not be viewed as evidence of association, since it is dictated by electroneutrality and is predicted by the Donnan or SDE models as well. Yet it does indicate that uptake of co-ions (anions) from a dilute solution will always be small, regardless of whether association is or is not included in the model.

The partitioning of co-ions A^- at small C_s may be obtained by expanding Eqs. (42b) and (46b), which gives.

$$S_A \approx S_0^2 C_s \frac{XK_{XMA}}{2 + K_{XM}K_{XM_2}^{-1/2}}(\mathrm{MA}); S_A \approx S_0^{3/2} C_s^{1/2} \frac{XK_{XMA}K_{XM}^{-1/2}}{2}(\mathrm{MA_2}). \quad (49)$$

These expressions may be compared with the SDE relation, Eq. (23), that predict that $S_A \approx S_0^2 C_s/X$ for MA and $S_A \approx S_0^{3/2}(C_s/X)^{1/2}$ for MA_2. It is seen that the SDE dependence of salt partitioning on C_s and S_0 is similar to Eq. (49), however, the membrane charge X is replaced with expressions that has an entirely different value and physical interpretation!

When C_s increases, the salt partitioning will first increase, following Eq. (49). However, upon further increase, the situation and observed trends may cross over to a different regime, whereby an increasing fraction of fixed charges may be converted to XMA or XM_2 triplets, as depicted in Figs. 5C and D. (Note that for MA salts, Fig. 5C, triplets are charged and for MA_2, Fig. 5D, they are neutral.) With increasing triplet formation, $\overline{n}_A$ and $\overline{n}_M$ may eventually saturate and salt partitioning may decrease, in total contradiction with SDE relations, but in qualitative agreement with RBS data by Zhang et al. [66].

It is important to stress that, in order that ion uptake approach such saturation, K_{XMA} and S_0 should be large enough to let ξ increase substantially within the realistic range of C_s (e.g., up to 1 M). Note that in the PM picture, K_{XMA} and S_0 are coupled through T^* in a way that, when one increases, another one decreases, which precludes crossover to a different regime (see Section 6). Therefore, possibility of another regime, suggested by experimental data, is only realistic when K_{XMA} (association) and S_0 (solvation) are *no more coupled* or are determined by different effective T^* values. Fig. 6 illustrates this point by plotting the ion uptake as a function of C_s according to Eqs. (47) and (48) for the same S_0, corresponding to $T^* = 0.15$, and a few values of K_{XMA}, corresponding to the same T^* and a few lower T^* values. For comparison, SDE predictions are shown as well. It is seen that curve 1 (the same T^* for both K_{XMA} and Γ_0) is qualitatively similar to SDE. However, as K_{XMA} is increasingly decoupled, a cross-over to a decreasing trend appears. It is also seen that MA_2 more readily departs from the SDE-like behavior than MA. The mechanisms that may cause such deviations from PM and decouple association from solvation are discussed in Section 6.4.

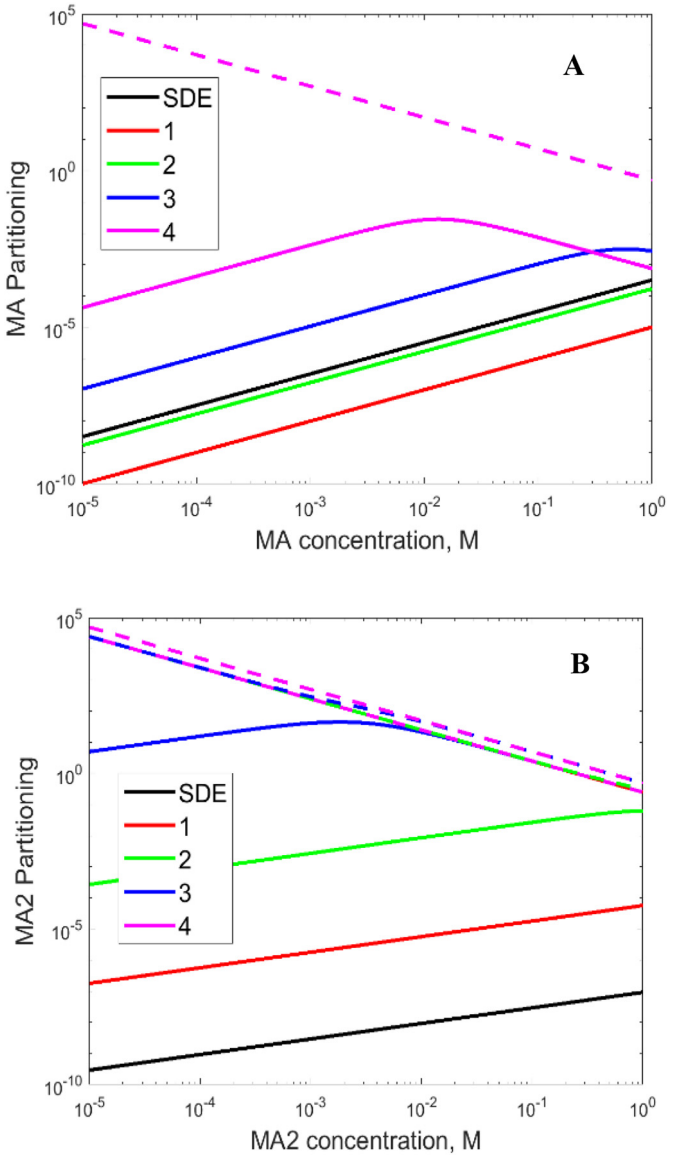

Fig. 6. Computed variation of co-ion (solid lines) and counter-ion (dashed lines) partitioning with salt concentration in solution: (A) MA salts, (B) MA_2 salts. Parameter used are $X = 0.5$ M, $b = 0.3$ nm, and $T^* = 0.15$ for computing salt injection coefficient S_0 using PM. Curves 1 to 4 correspond to PM values of association constants computed using $T^* = 0.15$, 0.10, 0.07, and 0.05 for fixed S_0. SDE predictions for the same S_0 are shown for comparison. Some dashed lines are not visible due to line overlap.

5.4. Ion mobility versus binding: trade-off relations in a charged membrane

5.4.1. Generalized interaction potential

Given PM may not supply accurate estimates of association constants (K values), they may have to be viewed as effective ion-specific parameters for practical modeling. However, such parametrization must not ignore the *inherent connection between ion binding and*

mobility, therefore both need to be analyzed in a consistent manner. To keep the relations reasonably general, we will first derive relations that relax the most problematic ingredient of PM, namely, purely electrostatic *short-range* interactions within the region $x < q$ defining the associated state.

Consider therefore a more general spherically symmetric dimensionless potential $U(x)$ that becomes predominantly electrostatic at distances $x >> b$, yet may involve non-PM shortest-range effects at distances $x \sim b$ with just two key features:

(a) the energy $U(b)$ at contact $x = b$ is strongly attractive, i.e., negative and large, thus $T^{\#} = 1/|U(b)|$ is small, and
(b) $U(x)$ rapidly decays away from $x = b$, with the attenuation length $|U(b)/U'(b)| = b^{\#}$ much smaller than the distance L between the binding sites (fixed charges).

These assumptions are consistent with the short-range nature of physical mechanisms that modify the inter-ionic Coulomb potential (see Section 6.3). Like for PM at small T^*, for such a potential the integrations involved in the derivation of both association constants and mobilities may be performed approximately.

5.4.2. Permeability of MA salts

First, define the self-diffusivity D_0 of a free ion in a uniform potential field, based only on its friction with the medium,. In a non-uniform potential field, featuring potential barriers and/or wells, the effective mobility or self-diffusivity D will have a different value, usually lower than D_0 [70,72]. Since the potential field depends on the type of associate, this effective value will differ for different types of associates, even for the same ion. If an ion forms different associates, the overall ion partitioning coefficients of the previous section will have to be split up to contributions by each associate, and the permeability P has to appropriately combine partitioning coefficients S and mobilities D (see Eq. (3)) of each type.

Derive first the contribution of XM pairs to M^+ permeability using the above generalized potential $U(x)$, starting from the generalized expression for association constant K_{XM}. The phase integral, Eq. (28), has to be evaluated now over the entire range $b < x < L/2$. At short distances $x \sim b$, it will still be dominated by the large and rapidly decaying exponential factor, while the other, more slowly changing terms may be replaced with their ground-state values at $x = b$. By approximating the potential as $U(x) \approx U(b) + U'(b)(x - b)$, Eq. (28) gives the pair constant

$$K_{XM} = 4\pi \int_b^{L/2} e^{-U(x)} x^2 dx \approx 4\pi b^2 e^{-U(b)+U'(b)b} \int_b^{q/2} e^{-U'(b)x} dx \approx K_2 = 4\pi b^2 b^{\#} T^{\#} e^{1/T^{\#}}. \quad (50)$$

When L is smaller or commensurate with λ_B and they are both much larger than $b^{\#}$, to a good approximation, the result is independent of the cell size L and K_{XM} is well approximated by the constant K_2, obtained by integration up to Bjerrum's cutoff $q = \lambda_B/2$ instead of $L/2$. It is easy to verify that for Coulomb potential $U(x) = -\lambda_B/x$, the result is identical to Eq. (28).

On the other hand, if $L >> q$, the region $q/2 < x < L/2$ with a negligible potential, i.e., $e^{-U(x)} \approx 1$, will add to K_{XM} roughly the volume $1/\tilde{X} \approx \pi(L^3 - q^3)/6$. For very small fixed charge density, $\tilde{X} \approx X << 1/K_2$, the value $1/\tilde{X} \approx 1/X$ represents the small-X limit for K_{XM}, while K_2 represents the opposite large-X limit of K_{XM}. To cover all cases, the two may be combined in one simple approximate relation $K_{XM} \approx K_2 + 1/X$. However, for values of X and T^* relevant here, this correction will be inessential and Eq. (50), i.e., $K_{XM} \approx K_2$ is adopted as an approximation below.

To compute the ion diffusivity consistent with the same potential $U(x)$, we will employ general relations presented by Lifson and Jackson [70]. They relate self-diffusivity in a cell to the average escape time $\bar{t}$ that takes the ion to reach the cell boundary. In the present case of an ion escaping from the ground state at $x = b << L/2$ to the cell boundary at $x = L/2$ in a spherically symmetric potential field $U(x)$, it takes the following form

$$\bar{t} = \frac{1}{D_0} \int_b^{L/2} dx' x'^{-2} \exp[U(x')] \int_b^{x'} dx'' x''^2 \exp[-U(x'')]. \quad (51)$$

The short-range region $x'' \sim b$ with the large and rapidly decaying exponential $\exp[-U(x'')]$ dominates the inner integral, which then depends weakly on x' for $x' >> b$. On the other hand, the term $\exp[+U(x')]$ in the outer integral is vanishingly small for $x' \sim b$. We then approximate the escape time for M^+ escaping an XM pair. i.e., interacting with remaining X^- fixed charge, as follows

$$\bar{t}_{M(XM)} D_{0M} = \int_b^{L/2} dx' x'^{-2} e^{U(x')} \int_b^{x'} dx'' x''^2 e^{-U(x')} \approx b^2 b^{\#} T^{\#} e^{-U(b)} \int_b^{L/2} dx' x'^{-2} e^{U(x')} \approx \frac{K_{XM}}{4\pi} \int_b^{L/2} dx' x'^{-2} e^{U(x')} \quad (52)$$

To evaluate the last outer integral, it may be reasonable to approximate $U(x)$ beyond the short range $x \sim b$ with the Coulomb potential $U(x) \approx -\lambda_B/x$, thereby

$$\bar{t}_{M(XM)} \approx \frac{K_{XM}}{4\pi D_{0M}} \int_{x=b}^{L/2} de^{-\lambda_B/x} = \frac{K_{XM}}{4\pi D_{0M} \lambda_B} \left(e^{-2\lambda_B/L} - e^{-\lambda_B/b} \right) \cong \frac{K_{XM}}{4\pi D_{0M} \lambda_B}. \quad (53)$$

In the last expression we dropped $e^{-\lambda_B/b} << 1$ and $e^{-2\lambda_B/L} \cong 1$ as inessential. As for Eq. (50), we also ignore the case of $L >> q$; otherwise, this would require adding to Eq. (53) a free-diffusion correction term approximately equal to $L^2/24$ in the small-X limit. Eq. (53) then expresses the large-X limit for $\bar{t}_{M(XM)}$.

The relations for binding of M^+ ions to or escaping from a charged triplet XM_2^+ are derived along the same lines. M^+ will now be in the field of a neutral pair XM. Beyond the shortest range $x \sim b$, the potential of the third ion may then be approximated by the ion-dipole potential $U_3(x) \sim -b\lambda_B/x^2$, assuming the XM dipole and M^+ are most favorably aligned. (A better approximation may have to average over different orientations, in which case U_3 will decay faster with x.) The result is then

$$K_{XM_2} \approx K_{XM} \int_b^{L/2} 4\pi x^2 e^{-U_3(x)} dx \approx K_3 = 10 b^2 b^{\#} T^{\#} e^{1/T^{\#}} K_{XM}. \quad (54)$$

Note the short-range interaction parameters $b^{\#}$ and $T^{\#}$ in general differ for K_2 and K_3. For instance, for the Coulomb potential, $T^{\#} \approx T^*$ for K_2, but $T^{\#} \approx 2\,T^*$ for K_3. Also, once again, we disregard the $1/X$ correction to the integral for $L >> q$, in which case $K_{XM_2} \approx K_3 + 2K_2/X + 1/X^2$ would be a simple approximate expression with correct small- and large-X limits. Ignoring this $1/X$ correction in Eq. (54) could be a cruder approximation than for Eq. (50), since the second M^+ ion does not bind as strongly as the first one, therefore $K_3 < K_2^2$. Besides, the minimum of $x^2 e^{-U_3(x)} \approx x^2 e^{b\lambda_B/x2}$ at the distance $q_3 \approx (b\lambda_B)^{1/2} = \lambda_B T^{*1/2}$ that separates the free and associated states for the third ion is smaller than Bjerrum's $q = \lambda_B/2$ for the second ion. Yet, q_3 is probably still commensurate with L, which justifies $K_{XM_2} \approx K_3$.

Derivation of the escape time of M^+ from a XM_2^+ triplet will follow Eqs. (51)–(53). In the last integral in Eq. (52) we may again neglect the shortest-distance contribution and drop the factor $\exp.[U_3(x)] \approx 1$ for larger distances, thus the outer integral is approximately $1/b$. This ultimately yields the escape time

$$\bar{t}_{M(XM_2)} \approx \frac{K_{XM_2}}{4\pi D_{0M} b K_{XM}}. \quad (55)$$

To exhaust all possibilities, note that M^+ may also be found in XMA triplets, however, it contributes negligibly to M^+ permeation. Indeed, M^+ ion escaping from an XMA triplet will leave behind a double-charged pair XA^{2-}, whose association energy is highly unfavorable hence $K_{XA} \approx 0$. The escape time $\bar{t}_{M(XMA)}$ is then very long, which means M^+ mobility within XMA is negligible.

Let us now combine all above contributions and compute the overall permeability of M^+. Consider its diffusion as a random Poisson process of ion hopping between different cells. Over a differential time dt, the fraction of ions that have escaped their original cells will be $dt/\bar{t}$. Note that the escape from the region of the strong attractive potential is slow, since the ion has to diffuse upfield, while the opposite downfield process, i.e., return to the ground state, is fast. Once an escaping M^+ ion enters the binding potential of a neighboring cell, X^- or XM, it will rapidly fall into the new ground state, XM or XM_2^+, respectively, completing a hop (displacement) by a distance L. The time of this downfall will be very short, therefore the escape time from the previous state $\bar{t}$ may reasonably approximate the average time of the entire hop.

For the sake of completeness, note this argument would not apply to the diffusion across the free-ion-like region in case $L >> q$, which would add to Eqs. (53) and (55) a term ~$L^2/24$. Since for an entire hop (and not just escape from the original cell) the free diffusion distance is doubled from $L/2$ to L, the added free-diffusion time for the entire hop will be 4 times larger, i.e. the total hop time would be roughly $\bar{t} + L^2/6$. As before, the $L^2/6$ correction is regarded inessential here, since, typically, $L \sim q$.

Note that some escapes towards the cell boundary will not result in a hop to a neighboring cell. If an escaping M^+ ion hits an XM_2^+ or XMA^- cell that – according to the assumptions made - is unlikely to accommodate another ion, the ion is most likely to return to the original ground state and end up with a zero displacement. As yet another approximation, let us ignore the correlations between neighboring cells and assume they are distributed randomly according to their equilibrium fractions. The average mean-square displacement (MSD) of an M^+ ion then has to weigh "successful" hops to XM or XM_2^+ cells (MSD = L^2) and "unsuccessful" ones, hitting XM_2^+ or XMA^- cells (MSD = 0), with appropriate equilibrium fractions. MSD will then increase with time approximately as

$$\frac{d\mathrm{MSD}_M}{dt} \approx \frac{1}{\bar{t}_M}\left(\frac{[X^-]+[XM]}{X}L^2 + \frac{[XM_2{}^+]+[XMA^-]}{X}0\right) = L^2\frac{1+K_{XM}[M^+]}{\xi}\frac{1}{\bar{t}_M}, \tag{56}$$

whence the mobility (self-diffusivity) is obtained using the Einstein relation as

$$D_M = \frac{1}{6}\frac{d\mathrm{MSD}_M}{dt} = \frac{L^2}{6}\frac{1+K_{XM}[M^+]}{\xi}\frac{1}{\bar{t}_M} \tag{57}$$

Finally, since M^+ ions can be released from states XM and XM_2^+, total average MSD of an M^+ ion has to add up MSDs for respective states weighed by their contributions to M^+ partitioning. Since MSD and D are linearly related (Eq. (57)), the macroscopic permeability P_M is obtained by similarly weighing ion diffusivities in different states, as follows

$$P_M = D_{M(XM)}S_{M(XM)} + D_{M(XM_2)}S_{M(XM_2)} \approx \frac{L^2}{6}\frac{[X^-]+[XM]}{X}\left(\frac{1}{\bar{t}_{M(XM)}}\frac{[XM]}{C_s} + \frac{1}{\bar{t}_{M(XM_2)}}\frac{2[XM_2{}^+]}{C_s}\right) \approx D_{0M}\frac{4(1+K_{XM}[M^+])\left(\lambda_B[M^+] + bK_{XM}[M^+]^2\right)}{L\xi^2 C_s}, \tag{58}$$

where $[M^+]$ and ξ are given by Eqs. (41) and (42c), and we also used Eqs. (53) and (55) and relation $X = 6/\pi L^3$. (Note the factor 2 before $[XM_2^+]$ because it contains two M^+ ions.)

The permeability of co-ions A^- is derived along the same lines. A^- is present only in XMA^- triplets and may escape only towards XM pairs. The expression for its escape time is then similar to Eq. (55),

$$\bar{t}_{A(XMA)} \approx \frac{K_{XMA}}{4\pi D_{0A} b K_{XM}}, \tag{59}$$

and its permeability is

$$P_A = D_{A(XMA)}S_{A(XMA)} \approx \frac{L^2}{6}\frac{[XM]}{X}\frac{1}{\bar{t}_{A(XMA)}}\frac{[XMA^-]}{C_s} \approx D_{0A}S_0^2 C_s\frac{4bK_{XM}^2[M^+]}{L\xi^2}. \tag{60}$$

Ultimately, the salt permeability is obtained using Eq. (9), $P_{MA} = 2(1/P_M + 1/P_A)^{-1}$.

5.4.3. Permeability of MA_2 salts

The permeability for MA_2 salts is derived similar to the previous section, assuming that X^-, XM^+ and XMA^0 are the dominant states. Opposite to MA salts, pairs are now charged and triplets are neutral. In this picture, the cations M^{2+} only hop from XM^+ to X^- cells, while anions A^- hop from neutral XMA triplets to XM^+ pairs, i.e., both ions escape from the field of a charge, not a dipole. Disregarding free diffusion ($L \sim q$), the average hop times are

$$\bar{t}_{M(XM)} \approx \frac{K_{XM}}{8\pi D_{0M}\lambda_B}, \tag{61}$$

$$\bar{t}_{A(XMA)} \approx \frac{K_{XMA}}{4\pi D_{0A}\lambda_B K_{XM}}, \tag{62}$$

and MA_2 counterparts of Eqs. (58) and (60) for ion permeabilities are

$$P_M = D_{M(XM)}S_{M(XM)} \approx \frac{L^2}{6}\frac{[X^-]}{X}\frac{1}{\bar{t}_{M(XM)}}\frac{[XM^+]}{C_s} \approx D_{0M}\frac{8\lambda_B}{L\xi^2 K_{XM}C_s}, \tag{63}$$

$$P_A = D_{A(XMA)}S_{A(XMA)} \approx \frac{L^2}{6}\frac{[XM^+]}{X}\frac{1}{\bar{t}_{A(XMA)}}\frac{[XMA]}{2C_s} \approx D_{0A}S_0^{3/2}\frac{4\lambda_B(K_{XM}C_s)^{1/2}}{L\xi^2}. \tag{64}$$

where ξ is given by Eq. (46c), K_{XM} and K_{XMA} given by Eqs. (50) and (54) with $K_2 \approx 4\pi b^2 b^{\#} T^{\#} e^{1/T^*}$ and $K_3 \cong 10 b^2 b^{\#} T^{\#} e^{1/T^*} K_2$, and we also used electroneutrality condition $[M^{2+}] = 1/K_{XM}$. As before, the short-range interaction parameters $b^{\#}$ with $T^{\#}$ in general differ for K_{XM} and K_{XMA}. For instance, their values for the Coulomb potential are $T^{\#} \approx T^*/2$ for K_{XM} and $T^{\#} \approx 2\,T^*/3$ for K_{XMA}. Ultimately, the salt permeability is $P_{MA_2} = 3(1/P_M + 2/P_A)^{-1}$.

5.5. Discussion: interpretation of permeabilities and limiting regimes

Expressions for P_M and P_A of the last sections are products of the free ion diffusivity D_0 and several dimensionless factors. Let us clarify their meaning, taking the Eq. (63) as an example, which we may rewrite as follows

$$P_M \approx D_{0M}\frac{8\lambda_B}{L}\left(\frac{[X^-]}{X}\right)^2\frac{[M^{2+}]}{C_s}, \tag{65}$$

The first factor, proportional to λ_B/L or b/L, reflects the average *non-uniformity of the long-range part* of the binding potential within a cell, which is what makes D deviate from D_0 over the long range. Thus, the ion-ion potential, which falls off more slowly, produces a larger factor

~λ_B/L than the ion-dipole potential that falls off faster and more weakly affects the long range (factor ~b/L). This factor is fairly similar for ions of the same charge and might be of limited importance for overall trends.

The second factor is the squared ratio $[X^-]/X = 1/\xi$, which is *the fraction of precursor cells*, capable of binding the mobile ion and also the cell type left behind after a hop. In a sense, it is analogous to the "porosity-tortuosity" factor in porous materials or normalized conductivity in conductor-insulator composites [73]. If it is small, there are fewer sites that can release the ion and fewer neighboring sites to hop to ("smaller porosity"), which also forces the ions to follow a more tortuous trajectory. This factor may become important when association is very strong and binding sites saturate, leaving only a few precursor cells.

The last, perhaps most important factor $[M^{2+}]/C_s$ should be understood as *the effective partitioning of free ions* regulated by association. In Eq. (63), it originates from the expression for the XM^+ pair concentration $[XM^+] \propto K_{XM}[M^{2+}]$. The constant K_{XM} enters ion diffusivity and partitioning in a reciprocal manner and ultimately cancels out in the final expression for permeability, leaving only $[M^{2+}]$.

We see that *the ion permeability in charged low-T^* membranes is mainly controlled by the free ion release from fixed charges and availability of precursor cells for ion hopping, both regulated by association.* This is principally different from the SDE model, where $[M^{2+}]$ is identified with the nominal charge X. Instead, in the present model, it is replaced with an *effective charge* that has a totally different value and physical meaning! Also note that the effective charge is ion-specific and differs for the permeability and partitioning (e.g., compare Eqs. (49) and (60)). This is fully consistent with much lower estimates of ion partitioning deduced form transport measurements, e.g., ion conductivity by impedance technique, as compared to direct ion-content measurements [55].

Similar to analysis of partitioning (Section 5.3), it is expedient to consider limiting regimes for permeability, starting from small C_s. For MA salts, both $[M^+]$ and ξ are about constant $[M^+] \approx {K_{XM_2}}^{-1/2}$ and $\xi \approx K_{XM}{K_{XM_2}}^{-1/2} + 2$ (cf. Eqs. (41) and (42c)). It is straightforward to see that Eqs. (58) and (60) predict a limiting behavior of P_M and P_A that has the same dependence on D_0, C_s and S_0 as SDE expressions for good co-ion exclusion $P_M = D_{0M}S_M \approx D_{0M}X/C_s$ and $P_A = D_{0A}S_A \approx D_{0A}S_0^2C_s/X$. This similarity obviously comes from the fact that in the low-C_s regime both the present model and SDE predict an about constant $[M^+]$, which inevitably results in a similar dependence on salt concentration for $[A^-] = S_0^2C_s^2/[M^+]$. This leads to a C_s-dependence qualitatively similar to SDE, different only in the effective values of membrane charge and ion mobility. Similarly, for MA_2 salts the limiting low-C_s values are $[M^{2+}] = K_{XM}^{-1}$ and $\xi = 2$ (Eqs. (45) and (46c)), thereby Eqs. (63) and (64) become reminiscent of the SDE expressions $P_M \approx D_{0M}X/2C_s$ and $P_A \approx D_{0A}S_0^{3/2}(C_s/X)^{1/2}$.

However, as C_s increases, the qualitative similarity between the present model and SDE may eventually disappear. This will occur when a significant fraction of fixed charges is converted to triplets, XM_2^+ and XMA^- for MA salts and XMA^0 for MA_2. In this regime, the co- and counter-ion concentrations in the membrane will become commensurate, resembling a "neutral membrane" regime of SDE with a negligible fixed charge (Section 5.2). The crucial difference is that the SDE model will tend to approach at high C_s a constant *ion partitioning* (Eq. (22)), while the present model will approach a constant *ion concentration* in the membrane thereby ion partitioning may decrease with C_s. The binding saturation and decreasing "porosity-tortuosity" factor may also add to such trend reversal. In addition, the co-ion permeability P_A could also become larger than P_M thereby the co-ion cedes to the counter-ion the control of salt permeability and its pH dependence, especially, for asymmetric MA_2 salts, for which cation binds more strongly. This is illustrated in Fig. 7 that plots the computed dependence of salt and co-ion permeability for MA and MA_2 salts. As in Fig. 6, S_0 is fixed for all curves by setting $T^* = 0.15$ in Eq. (33), but several progressively smaller values of T^* are used to compute association constants in order to allow for their possible non-PM

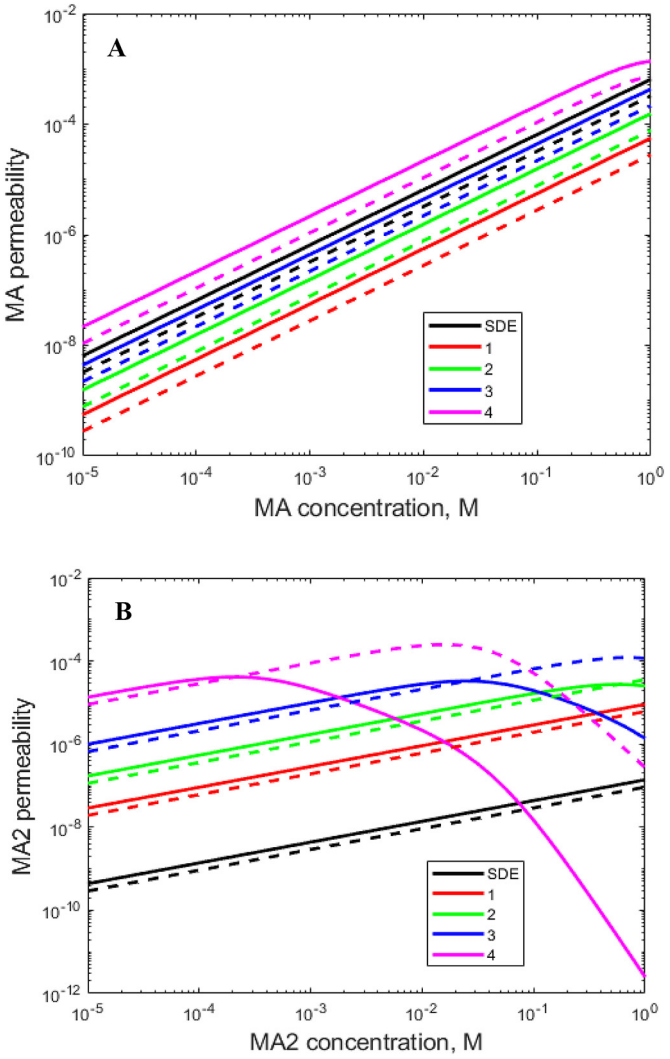

Fig. 7. Computed variation of salt (solid lines) and co-ion (dashed lines) permeability with salt concentration in solution: (A) MA salts, (B) MA_2 salts. Permeabilities are normalized to D_0, assumed to be the same for co- and counter-ions. Parameter used are $X = 0.5$ M, $b = 0.3$ nm, and $T^* = 0.15$ for computing salt injection coefficient S_0 using PM. Curves 1 to 4 correspond to PM values of association constants computed using $T^* = 0.15$, 0.12, 0.10, and 0.08 for fixed S_0. SDE predictions for the same S_0 are shown for comparison. In panel B, dashed lines moving above the solid lines indicate that salt permeability becomes dominated by M^{2+} counter-ions.

behavior (Section 6). It is seen that, compared to MA salts (Fig. 7A), MA_2 salts are more prone to transitioning a qualitatively different behavior, when association is determined by the same T^* (Fig. 7B). This could explain both the decreasing dependence of P_s on C_s for $CaCl_2$ and $MgCl_2$ salts and the unexpected effect of pH on $CaCl_2$ permeability, highlighted in Fig. 2. To demonstrate that transition to a different high-C_s regime, explaining experimental results, requires association constants far above PM predictions, the next section analyzes what is expected within PM.

6. Primitive model and beyond

Previous section presents general relations that contain ion- and membrane-specific association constants (K) and affinities (k and, ultimately, S_0). In general, PM may be a poor model to predict these parameters, since they may involve physical effects inherently absent in PM. However, it would be instructive to examine PM predictions, to highlight its limitations as well. For numerical estimates, we will use below a "toy model" that assumes that all ions, including fixed charges,

are of equal diameter b and the membrane is a dielectric continuum with a fixed Bjerrum length λ_B and $T^* = b/\lambda_B$. We presume $b = 0.3$ nm ($b^3 = 0.016$ M^{-1}) reasonably represents many ions as well as fixed charged groups, while $T^* = 0.15$ ($\varepsilon \approx 30$ and $\lambda_B \approx 2$ nm for above b) and $X = 0.5$ M and $L = (6/\pi X)^{1/3} \approx 1.85$ nm, commensurate with λ_B, are representative of NF membrane characteristics. In fact, the average dielectric constant for the selective layer must be in the range 6 to 10, i.e., $T^* = 0.04$ to 0.06, based on water fraction in the membrane and structure-property-composition correlations [74–76], as well as impedance measurements [54]. However, we prefer $T^* = 0.15$ as a conservative estimate that is probably more characteristic of the water in the NF nanopores, i.e., the medium solvating the ions [53]. For simplicity, we also ignore steric exclusion ($\Phi = 1$), which may somewhat overestimate S_0.

6.1. Degree of association and co-ion partitioning

To appreciate the extent of association, let us first estimate what fraction of the fixed charges remains in the dissociated X^- form. In terms of the one-site grand partitioning function ξ (Eqs. (38) or (44)), this fraction is simply $1/\xi$, but the numerical value depends greatly on the salt type. In all cases, ξ increases with salt concentration, therefore the low-C_s limit of ξ gives the maximal possible fraction. For MA salts this gives

$$\left(\frac{[X^-]}{X}\right)_{max} = \frac{1}{\xi_{min}} = \frac{1}{2 + K_{XM}\left(K_{XM_2}\right)^{-1/2}} \approx \frac{1}{2 + T^{*-1/2}e^{1/4T^*}}, \tag{66}$$

where we used Eqs. (29) and (30) in the last expression. For $T^* = 0.15$, the result is that at most only 6.4% of the nominal fixed charge is dissociated. As long as the fraction of [XMA$^-$] triplets is negligible (as expected for dilute solutions), about the same fraction will be converted to XM_2^+ triplets, while the remaining 87.2% will be neutral XM pairs, as schematically shown in Fig. 5A.

The situation will be quite different for MA_2 salts, due to double charge of the cation. Here, the low-C_s limit is

$$\left(\frac{[X^-]}{X}\right)_{max} = \frac{1}{\xi_{min}} = \frac{1}{2}, \tag{67}$$

which corresponds to 50% dissociated charges and 50% XM^+ pairs, when the fraction of neutral XMA triplets is negligible, as illustrated in Fig. 5B. This result does not depend on T^*, as long as it is low enough to keep λ_B larger or commensurate with the cell size L.

When salt concentration C_s increases, more triplets will form and the above numbers will decrease. The content and permeability of A^- ions will first vary in the manner of SDE model in the good co-ion exclusion regime, with an appropriate effective fixed charge replacing X (see Section 5). The next question is whether, within practical C_s range, this behavior may eventually cross over to the high-C_s regime, when the fraction of XMA triplets is no more negligible. It is straightforward to see from Eq. (43) that, for MA salts, it would require that $K_{XMA}(S_0C_s)^2$ be of the order 1. We may use PM relations, Eqs. (30) and (33), to convert this condition to the following one

$$K_{XMA}(S_0C_s)^2 \cong 10^2\left(b^3C_s\right)^2 T^{*3}e^{-1/2T^*} \sim 1. \tag{68}$$

To satisfy this condition for $b = 0.3$ nm and $T^* = 0.15$, C_s will have to be about 560 M.

Similarly, Eq. (47) along with PM relations, Eqs. (29), (30) and (33), yield the analogous condition for MA_2 salts

$$K_{XMA}\left(\frac{S_0^3C_s^3}{K_{XM}}\right)^{1/2} \cong 10^{3/2}\left(b^3C_s\right)^{3/2} T^{*5/2}e^{-1/2T^*} \sim 1, \tag{69}$$

which requires even higher $C_s \sim 1300$ M. These concentrations are far beyond the practical C_s range, usually, about 10^{-4} to 1 M. PM then rules out that the low-C_s regime ever crosses over to a different one, unless the terms $K_{XMA}S_0^2$ in Eq. (68) or $K_{XMA}(S_0^3/K_{XM})^{1/2}$ in Eq. (69) exceed the PM predictions by at least 3–4 orders of magnitude. Plots in Fig. 6 illustrate this point and show behavior qualitatively different from SDE, only when T^* used to compute association constants is reduced to about half the value for S_0, which is equivalent to about 3–4 orders of magnitude discrepancy.

Nevertheless, RBS partitioning data reported by Zhang et al. for RO membranes [66], do show unexpectedly large partitioning, commensurate for co- and counter-ions and decreasing with salt concentration. Based on Eqs. (47) and (48), such behavior is only possible, when a significant fraction of fixed charged is converted to XMA triplets or still larger aggregates. Even if these results might be amenable to a different interpretation and the actual deviations from PM might not be as large, large deviations are indeed possible and likely, as discussed in Section 6.4. Even if they are still insufficient to change the low-C_s trend for partitioning, they can more readily affect the salt permeability (see next).

6.2. Ion permeability: low- and high-concentration regimes

As shown in the previous section, PM anticipates a negligible fraction of XMA triplets, in which case equations simplify significantly, since [M] and ξ are well approximated by their constant minimal values. This defines the low-C_s regime that resembles the charged membrane regime of SDE. For SDE, one may anticipate a crossover to a different regime (form charged to neutral membrane) at the point where extrapolated low-C_s trends of P_A and P_M meet. We may apply the same principle to the present model and compute the ratio of P_A and P_M contributions to P_s, i.e., P_A/P_M for MA and $P_A/2P_M$ for MA_2 salts to see when they equal 1. To facilitate calculations, also assume $D_{0A} = D_{0M}$.

For MA salts, we obtain from Eqs. (58) and (60)

$$\begin{aligned}\frac{P_A}{P_M} &\approx \frac{bS_0^2C_s^2K_{XM}^2[M^+]}{\lambda_B[M^+] + bK_{XM}[M^+]^2} \approx \frac{S_0^2C_s^2K_{XM}^2}{\lambda_B/b + K_{XM}K_{XM_2}^{-1/2}} \\ &\approx \left(b^3C_s\right)^2 \frac{10^2T^{*2}}{T^{*-1} + T^{*-1/2}e^{1/4T^*}}.\end{aligned} \tag{70}$$

For $b = 0.3$ nm and $T^* = 0.15$, this equals 1 at $C_s \approx 185$ M. This is obviously still beyond the realistic range of C_s, but is not as much off-range as for partitioning. Cross-over to high-C_s regime of permeability would require an order-of-magnitude smaller deviations from PM than for partitioining. The required change would be mostly related to parameters in the numerator of Eq. (70), since denominator would change more slowly. Therefore, the quantity S_0K_{XM} would have to increase relative to PM value by 2–3 orders of magnitude, which may be realistic (see Section 6.4).

Similar analysis for MA_2 salts leads to the following expression

$$\frac{P_A}{2P_M} \approx \frac{(S_0K_{XM}C_s)^{3/2}}{4} \approx \frac{1}{4}\left(5T^*b^3C_s\right)^{3/2}. \tag{71}$$

It gives $C_s \approx 210$ M for the cross-over concentration at which extrapolated P_A equals P_M. This value would also require a 2–3 orders of magnitude increase of the product S_0K_{XM} above PM predictions, which is more likely for divalent ions (see Fig. 7).

6.3. Permeability and physical characteristics of NF and RO membranes

Another, more straightforward way to see whether PM is consistent with actual membrane characteristics is to look at the absolute values of permeability. NF270 or its predecessor NF200 are typical NF

membranes, for which dominant role of dielectric exclusion is well-established [44–46,77] and permeability data as well as physical characteristics are available. To estimate their dielectric characteristics, we may use more "regularly" behaving permeability of NaCl (see Fig. 2A). The experiments show that NaCl permeability of NF270 is $\omega_s \approx 2 \times 10^{-5}$ m/s at $C_s = 0.1$ M [4]. Given the active layer thickness is about 20 nm [76], we estimate $P_s \approx 4 \times 10^{-13}$ m^2/s. A similar value of P_s is obtained for twice as thick NF200 membrane, suggesting this is an intrinsic material characteristics [35,76].

Following PM analysis above, we identify P_s with P_A or, more accurately, $P_A \approx P_s/2 \approx 2 \times 10^{-13}$ m^2/s. We may then use Eq. (60) and PM relations, Eqs. (29) and (33), for association constants and salt injection coefficient and apply low-C_s values $\xi \approx K_{XM}[M^+]$ and $[M^+] \approx {K_{XM_2}}^{-1/2}$, as follows

$$P_A \approx D_{0A} S_0^2 C_s \frac{4bK_{XM}^2[M^+]}{L\xi^2} \approx D_{0A} S_0^2 C_s K_{XM_2}^{1/2} \frac{4b}{L} \approx \frac{4b}{L} D_{0A} \left(10 b^3 C_s\right) T^{*3/2} e^{-5/4T^*}. \tag{72}$$

For the water volume fraction in the membrane $\phi_w \approx 0.25$, tortuosity about 1.8, and membrane pore size about 0.35 nm, D_0 of Cl^- is estimated to be about 10^{-10} m^2/s [35]. Unfortunately, the representative values $T^* = 0.15$, $b = 0.3$ nm, and $L = 1.8$ nm produce $P_A \approx 1.5 \times 10^{-17}$ m^2/s, four orders of magnitude lower than the experimental value. Such a large discrepancy points to either inadequate values of parameters or a failure of the PM model.

Different methods used to estimated membrane charge produce fairly consistent values of $X \sim 0.5$ M [50,51,66–69] and excessive adjustments of the ion size b would be unphysical. Reasonable adjustments of these parameters reduce disagreement only marginally. It would then be more reasonable to increase T^*, but the one used is already quite large and about an order of magnitude discrepancy remains even if $T^* = 0.42$ of bulk water is used. The discrepancy then most likely comes from the model itself and, in particular, from the expression for the *effective membrane charge* that replaces X in the SDE expression $P_A \approx D_{0A} S_0^2 C_s / X$.

In order to examine what value of the effective charge could match the experimental permeability, we start from its lower bound $X = 0$, i.e., the neutral membrane. In this case X drops out of the equations and the appropriate expression is $P_A \approx D_{0A} S_0 = D_{0A} e^{-1/T^*}$ (see Section 5.2). Using $T^* = 0.15$, we obtain $P_A \approx 1.3 \times 10^{-13}$ m^2/s, fairly close to the experimental value. This suggests the membrane essentially behaves as neutral, despite overwhelming evidence that it has a substantial content of ionizable group. A similar observation was made for many other ion-polymer systems [37], suggesting that NaCl permeability may be no more "regular" than $CaCl_2$.

Once again, the most likely explanation is a non-PM behavior whereby a significant fraction of fixed charges in the membrane is converted to triplets. Indeed, when $K_{XMA}(S_0 C_s)^2 >> 1$, the free ion partitioning will approach (cf. Eqs. (39) and (41))

$$\frac{[M^+]}{C_s} \approx S_0 \frac{K_{XMA}}{K_{XM_2}}, \quad \frac{[A^-]}{C_s} \approx S_0 \frac{K_{XM_2}}{K_{XMA}}. \tag{73}$$

The resulting permeability would be barely distinguishable from the genuine neutral membrane behavior, for which $[M^+]/C_s = [A^-]/C_s = S_0$, especially, if K_{XMA} and K_{XM} are not too different. (In fact, they are identical in our toy PM model.) In Fig. 2A, NaCl does not plateau at high concentration, but the slope (exponent) is noticeably smaller than 1 [14], suggesting a possible approach to this regime. A slope smaller than the Donnan-exclusion slope was also reported for other ion-polymer systems [37]. Since such behavior is precluded by PM (Section 6.1), this result is yet another indication that PM may grossly underestimate the strength of association and overestimate the effect of fixed nominal charge, as discussed next.

6.4. Beyond the primitive model

PM supplies a reasonable starting point for analyzing thermodynamics and dynamics of solvation and association. Yet, even in simple liquids, it is a crude model and significant deviations are not uncommon [8,10]. For instance, they often lead to unphysical b values, smaller than the sum of bare ionic radii, i.e., PM underestimates the strength of association by ignoring various short-range effects that enhance association.

First, removal of solvating molecules from the space between the ions, i.e., partial overlap and shedding of ion hydration shells upon pairing, may enhance association quite significantly [10]. A direct effect comes from the reduced inter-ion distance b and more vacuum-like space between the ions, which is equivalent to ε and T^* becoming effectively smaller. However, in a polymeric membrane phase, there may also be a strong indirect effect coming from the fact that the polymeric membrane phase contains only a fraction of water, $\phi_w << 1$. To keep the ion content low, the reduced entropy per water molecule within the membrane, $\sim k_B \ln \phi_w$, has to be exactly balanced by the swelling pressure exerted by the matrix on water molecules [78]. The same pressure is exerted on ion pairs, which means that, by shedding a water molecule, an ion-pair reduces its free energy by about $k_B T \ln \phi_w$. Ultimately, release of m water molecules will increase the association constant from its purely electrostatic value K_{el} to.

$$\ln K \approx \ln K_{el} - m \ln \phi_w \text{ or } \quad K \cong K_{el}/\phi_w^m. \tag{74}$$

Since m between 1 and 3 per ion, i.e., 2 to 6 per ion-pair, is common for ion association in water [8], we may take $m \sim 2$ to 3 *per ion-pair* as a fairly likely number in a membrane. For $\phi_w \sim 0.1$–0.2 reported for NF and RO membranes [35,74,79,80], this increases K by as much as 2–3 orders of magnitude.

One may also anticipate that the low-dielectric environment of the membrane phase and enhanced electrostatics may increase association energy by promoting a partly covalent binding. The magnitude of such effect in polymeric membranes has to be clarified in future research. However, ab initio calculations for a NaCl pair in vacuum showed that at $b = 0.4$ nm the extra non-Coulomb binding energy may be as much as 10 $k_B T$ [56], which, according to Eq. (50), would increase the association constant of an ion pair by a factor $\sim e^{10}$, i.e., by another 3–4 orders of magnitude.

Yet another factor may be the dielectric micro-heterogeneity of the membrane, composed of dense polymeric matrix and water-filled nanopores [61,81–83]. In such systems, just like in many biopolymers, the local dielectric constant next to non-polar monomer units bearing a fixed charge may be lower than the macroscopic average [84], enhancing interaction beyond average-based PM predictions.

All above effects highlight great sensitivity of the association energy to the microenvironment, especially, the small space between interacting ions. In contrast, ion self-energy and salt injection coefficient S_0 are controlled by a more extended volume and may be less sensitive to microenvironment, as long as the scale of dielectric heterogeneity is commensurate with ion size [44,45]. The latter condition is reasonably satisfied in NF and RO membranes, with pore radii of about 0.2–0.4 nm. The aforementioned effects may then increase association without affecting solvation (salt injection) as much. Overall, this decoupling of association and solvation is what may lead to a behavior ruled out by PM, in particular, enhanced formation of XMA triplets and still larger associates, resulting in effective neutralization of the membrane charge and non-trivial behavior of salt permeability.

7. Competitive ion binding in a charged membrane

In many practical situations, the solution contains several ions that may compete for binding to the fixed charges. For instance, consider a feed solution containing two 1:1 salts MA and NA with a common

anion, such as NaCl and KCl. Considering only pairs for simplicity, ξ will become (cf. Eq. (38))

$$\xi = \frac{1}{X}\left([X^-] + \left[XM^0\right] + \left[XN^0\right] + \ldots\right) = 1 + K_{XM}[M^+] + K_{XN}[N^+] + \ldots. \tag{75}$$

Including triplets is straightforward but tedious, as it has to consider five different species, XM_2^+, XN_2^+, XMN^+, XMA^-, and XNA^-. Yet, in principle, given all required association constants, ion affinities and the solution composition, i.e., C_M, C_N, and $C_A = C_M + C_N$, free ion concentrations $[M^+]$, $[N^+]$, and $[A^-]$ may be found by combining total electroneutrality and two equilibrium relations for MA and NA salts (Eq. (39)), from which ξ and all other quantities may be computed. Fortunately, the expressions for co-ions are compact; in particular, partitioning will be (cf. Eq. (47))

$$S_A = \frac{[XMA] + [XNA]}{C_A} = X\frac{K_{XMA}S_{0MA}^2 C_M + K_{XNA}S_{0NA}^2 C_N}{\xi}, \tag{76}$$

and co-ion permeability as (cf. Eq. (60))

$$P_A = \frac{L^2}{6C_A}\frac{[XM] + [XN]}{X}\left(\frac{[XMA^-]}{\bar{t}_{A(XMA)}} + \frac{[XNA^-]}{\bar{t}_{A(XNA)}}\right) \approx \frac{4D_{0A}b}{L}\frac{K_{XM}S_{0MA}^2 C_M + K_{XN}S_{0NA}^2 C_N}{\xi}, \tag{77}$$

where in the last expression we dropped for simplicity the factor $([XM] + [XN])/X$, though this may significantly overestimate permeability. Note that the expression for S_A, Eq. (76), contains triplet constants K_{XMA} and K_{XNA} in the denominator, while that for P_A (Eq. (77)) contains pair constants K_{XM} and K_{XN},

As an important example, consider a somewhat special situation of NaCl permeation when Na^+ competes with proton H^+. H^+ affinity to aromatic polyamide was found to be 10^3 times larger than that of Na^+, i.e., S_{0HCl}/S_{0NaCl}~10^3 [19,85,86]. Furthermore, H^+ permeability in a polyamide RO membrane was estimated to be at least 10^5 times larger than permeability of NaCl [19,85,86]. The latter may partly come from the large S_{0HCl} as well as exceptionally high mobility (D_0) of the proton, but it may also reflect a large binding constant of proton K_{XH} (see Eq. (78)). When NaCl concentration is low enough, the H^+ terms in the numerator of Eqs. (76) and (77) may outcompete the Na^+ terms, even if proton concentration is orders of magnitude lower, i.e., pH is close to neutral. This should weaken the dependence of the Cl^- partitioning and permeability and, ultimately, NaCl permeability on the salt concentration. The permeability will then not decrease as expected for a single salt, when NaCl concentration is reduced further, as indeed observed in Fig. 2A. Essentially, proton increases salt partitioning and permeation, through its own absolute permeation rate may be low due to low H^+ concentration.

Analogous though more complex competition may occur in mixtures of a divalent and a monovalent cation salts with a common anion, $M^{2+}A_2^-$ and N^+A^-, for instance, $CaCl_2$ and NaCl. Up to triplets, ξ would include six terms, as follows

$$\xi = 1 + K_{XM}\left[M^{2+}\right] + K_{XN}[N^+] + K_{XN_2}[N^+]^2 + K_{XMA}\left[M^{2+}\right][A^-] + K_{XNA}[N^+][A^-]. \tag{78}$$

Two equilibrium relations, Eqs. (39) and (44), connect free ion concentrations $[M^{2+}]$, $[N^+]$, and $[A^-]$ in the membrane to the solution composition, while the electroneutrality requires that all terms at r.h.s. of Eq. (78) multiplied by their charges sum up to zero. In this way, closed (though somewhat lengthy) analytical formulae may be derived for all relevant quantities as a function of C_M, C_N, and $C_A = 2C_M + C_N$. For instance, free A^- partitioning will be

$$\frac{[A^-]}{C_A} = \left[\frac{K_{XM}S_{0,MA_2}^3 C_M + K_{XN_2}\left(S_{0,NA}^2 C_N\right)^2}{1 + K_{XNA}S_{0,NA}^2 C_A C_N}\right]^{1/2}. \tag{79}$$

When the ratio of C_M to C_N varies in a way that C_A stays constant, as in Fig. 2B, the terms that involve more strongly associating M^{2+} will dominate Eq. (79), except when the fraction of M_2^+ in solution becomes negligible. These terms will control ion partitioning and permeation, therefore, as long as C_M and C_N are commensurate, anion permeability approximates as (cf. Eq. (60))

$$P_A = \frac{L^2}{6C_A}\frac{[XM^+] + [XN]}{X}\left(\frac{\left[XMA^0\right]}{\bar{t}_{A(XMA)}} + \frac{[XNA^-]}{\bar{t}_{A(XNA)}}\right) \approx 4D_{0A}\frac{\lambda_B}{L}\left(\frac{[XM^+]}{X}\right)^2\frac{[A^-]}{C_A}. \tag{80}$$

It is straightforward to verify that the variation of P_A with composition will be slow, except when $[M^{2+}]$ is negligible. This will be especially true when there is a substantial triplet formation, in which case the last two factors in Eq. (81) tend to compensate each other. Since A^- permeation controls NA salt permeability, as suggested by the effect of pH in Fig, 2A, the NA permeablity will vary slowly with composition, up until M^{2+} fraction in solution becomes negligible. This may explain the results for NaCl in Fig. 2B.

On the other hand, the permeability of M^{2+} approximates as (cf. Eq. (63))

$$P_M = \frac{L^2}{6C_M}\frac{[X^-]}{X}\frac{[XM^+]}{\bar{t}_{N(XM)}} = 8D_{0A}\frac{\lambda_B}{L}\Gamma_{0,MA_2}^3\left(\frac{[X^-]}{X}\right)^2\left(\frac{[A^-]}{C_A}\right)^{-2}, \tag{81}$$

Since each of the last two terms now decrease when the M^{2+} fraction in solution increases, P_M will show a monotonic decrease with C_M. The effect of pH in Fig. 2B indicates that $CaCl_2$ permeability is controlled by Ca^{2+} permeation, therefore the observed variation for $CaCl_2$ permeability in mixed solution in Fig. 2B is consistent with Eq. (81). Once again, such unusual behavior requires an exceptionally strong association of Ca^{2+} with fixed charges, far beyond PM predictions.

8. Summary and outlook

The classical mean-field models of ion transport in membranes were originally devised for systems with weak ion-ion interactions, i.e., high-T^* limiting regime in the present terminology. Their characteristic feature is delocalized behavior (nearly free translation) of mobile ions and direct coupling between ion partitioning and permeation, which permits a straightforward break up of permeability to diffusion and sorption factors. Unfortunately, low-dielectric properties of many ion-rejecting and ion-selective membranes are incompatible with this simple picture and represent an opposite regime, close to the low-T^* limit.

Admittedly, with a few exceptions [4,12,17,87], the models of NF over last four decades has been largely developed around the view of the membrane as an array of nanopores [7,23–37], rather than a homogeneous medium in the manner of this work. However, closer inspection reveals that nanopore models largely retain the mean-field character of SDE. Even if the local potential in a nanopore is allowed to vary radially, the common use of a uniform wall surface charge density ignores the discrete nature of the fixed charges and essentially averages the potential in the dimensions parallel to the pore walls. The resulting solution, usually obtained by solving the PB equation within the pore, is then a radially averaged mix of the regimes described by the SDE model. Since for pore sizes of NF and RO, typically well under 0.5 nm, the low dielectric matrix still strongly affects the ion self-energy [44,45], the

use of high-T^* mean-field relations such as the PB equation faces the same objections as for a dielectrically homogeneous membrane.

As more appropriate for the low-T^* regime, the chemical-model-like description developed here introduces association as a key element. In this picture, fixed charges bind mobile ions, which lowers the effective membrane charge and reduces ion mobility, strongly modifying the relations between ion partitioning, mobility and permeability. Ultimately, the model shows that the much reduced free ion content in the membrane and the fraction of sites available for binding mobile ions rather than total ion content is what determines the salt permeability. This leads to a puzzling behavior of permeability, precluded by mean-field models but observed in experiments, such as salt permeability decreasing with concentration or controlled by counter-ions. This is also fully consistent with largely discrepancies between estimates of ion partitioning obtained by direct ion-count methods and by impedance-based membrane conductivity measurements [55].

Another conclusion is that simple continuum PM electrostatics appears to fail and underestimate the strength of ion association. The molecular structure of the medium solvating the ions is a likely reason and it can manifest itself in several possible mechanisms, all of which may enhance association by orders of magnitude. This may permit formation of triplets, strongly suggested by experimental data but ruled out by PM calculations. This may also allow ion condensation to much larger associates, ignored for simplicity in the present model, which may explain surprisingly large ion partitioning of both co- and counter-ions in RO membranes reported by Zhang et al. [66]. Since PM electrostatics is also the inherent basis for many other models of membrane transport, in particular, the nanopore models, its accuracy in these cases may be questioned as well.

The present model is obviously crude and should best be viewed as representing the limiting regime that approximates low-T^* membranes in the same sense, as the Donnan or SDE models do for well-hydrated high-T^* systems. The actual behavior may be intermediate to these two limiting regimes and future refinements may need to address this fact. For instance, they may need to consider the small-X corrections to association constants and escape time discussed Section 5.4 in relation to Eqs. (51), (54) and (57), which may bridge between small- and large-X regimes. One may also need to address the fact that the potential at the cell boundaries imposed by adjacent cells in Fig. 4 might not be negligible, which may have to be considered in more complete calculations. However, the largest challenge towards predictive modeling will be thorough quantitative understanding of non-PM aspects of association and solvation in membranes, as well as in nanopores.

In absence of a predictive theory, practical modeling of ion separations using the present approach will admittedly need a large number of parameters. In general, they will have to be membrane- (ε, X etc.) and ion-specific (r, k, K), which could require a large amount of high-quality experimental data, especially, for multi-ion solutions. This is however true for all models proposed so far, which need to utilize various ad hoc adjustments to the membrane or ion characteristics to obtain reasonable fits [88]. In this respect, a sounder physical basis of the present model could eventually help reduce the complexity and number of adjustable parameters. For instance, appropriate "mixing rules" could make a few parameters evaluated from experiments with single salts applicable to mixed solutions and properly link the model to structural characteristics, which is where previous models have failed so far. The resulting relation would also be capable of describing the observed trends, which previous models were unable to explain.

A viable and attractive alternative to experimental parameters evaluation would be molecular (MD) and quantum (ab initio) molecular dynamic (QMD) simulations. MD simulations have already shown much promise in RO and NF membrane research, e.g., they were capable of correctly predicting the water permeability and analyzing membrane interaction with foulants and neutral permeants using representative model polyamide structures [83,89–97]. Unfortunately, there are fewer results that address thermodynamics and transport of ions in polyamide [61,95,98,99]. Estimates for ions also may not readily extrapolate to the macroscale, since the membrane phase contains relatively few ions and estimated characteristics are highly sensitive to structural heterogeneities [61]. Nevertheless, the author is optimistic that future development of dedicated MD model systems and methods may help overcome these difficulties and quantify the extent of ion solvation and degree of association, including solvent-structure and related effects. Similarly, QMD simulation may clarify and quantify the role of quantum effects, possibly involved in ion binding and diffusion, especially, for ions such as H^+ and OH^- [100,101].

Finally, the author would like to credit the recent insightful work by Yaroshchuk et al. [6] who also noticed disagreements between its predictions and experiments and questioned the view of membranes or nanopores as a continuum. These authors drew attention to the fact that, given NF membranes are very thin, electroneutrality may be violated over a substantial part of their thickness, which offers an alternative explanation to some of the experimental observations discussed here. Nevertheless, since their analysis still relies on the mean-field relations, the questions of applicability and possible relation between the two approaches is open and will have to be clarified in the future.

Glossary and symbols

Variables

a	solute activity, $1/m^3$
A	Peclét coefficient, s/m
b	inter-ionic distance at contact, m
$b^{\#}$	attenuation length of short-range potential, m
c	concentration in the membrane, $1/m^3$
C	concentration in solution, $1/m^3$
C'	upstream (feed) solution concentration, $1/m^3$
C''	downstream (permeate) solution concentration, $1/m^3$
$\mathbf{C}$	concentration vector containing concentrations of all solutes, $1/m^3$
D	diffusion coefficient, m^2/s
e	electron charge, C
f	friction coefficient, J s/m^2
g^E	dimensionless excess free energy of an ion (in k_BT units)
I	electric current density, A/m^2
J	solute flux, $1/(m^2\ s)$
J_V	volume flux, m/s
$\mathbf{J}$	flux vector containing fluxes of all solutes, $1/m^3$
k	affinity coefficient
k_B	Boltzmann constant, J/K
K	association constant, m^3 (pairs) or m^6 (triplets)
L	average spacing between ions or fixed charges, m
MSD	mean-square displacement, m^2
$\overline{n}$	average number of ions per fixed charge
P	intrinsic (thickness normalized) permeability, m^2/s
Pe	Peclét number
p	probability of finding an ion in a given volume
q	distance separating free and associated states, m
Q	factor correcting association constant relative to the ground-state expression
r	ion radius, m
s	dimensionless entropy per solute (in k_B units)
S	solute partitioning (sorption) coefficient
t	time, s
$\overline{t}$	average escape time for an ion, s
T	absolute temperature, K
T^*	reduced temperature for Coulomb interactions
$T^{\#}$	reduced temperature for short-range interactions
U	dimensionless pair-wise interaction energy (in k_BT units)
W	dimensionless solvation energy (in k_BT units)

x	normal (across the membrane) or radial (around a charge) coordinate, m
$\bar{x}$	normal coordinate scaled by membrane thickness
X	fixed charge density, $1/m^3$
z	absolute ion charge in units of electron charge e
α_n	dimensionless ground-state energy of n-plet (in T^* units)
γ	activity coefficient
Δx	membrane thickness, m
ε	dielectric constant
ε_0	permittivity of vacuum, C/(V m)
θ_n	ratio of association constants of successive n- and $(n-1)$plet
Θ	ratio of concentrations of successive homologue associates
λ_B	Bjerrum length, m
λ_D	Debye length, m
μ	dimensionless chemical potential (in k_BT units)
ξ	one-site grand partition function
σ	reflection coefficient
ϕ	volume fraction
φ	dimensionless electric potential (in k_BT/e units)
φ_D	dimensionless Donnan potential (in k_BT/e units)
Φ	Ferry steric exclusion factor
ψ	dimensionless electrochemical potential (in k_BT units)
ω	diffusion permeability, m/s
[…]	concentration of respective species in the membrane phase, $1/m^3$

Indices

i, j	ions or solutes i, j
n	n-plet
s	salt
w	water
2, 3, …	pairs, triplets, …
+, −	cation, anion

Ionic species

A	mobile (salt) anion
M	mobile (salt) cation
X	fixed charge

Declaration of competing interest

The author declares that he has no known competing financial interests or personal relationships that could have appeared to influence the work reported in this paper.

Acknowledgments

The financial support by Israel Science Foundation (grant #1152/11) and by a grant 2016627 of the United States-Israel Binational Science Foundation (BSF), Jerusalem, Israel, jointly with the United States National Science Foundation (NSF) is acknowledged. The author thanks Ora Kedem, Andriy Yaroshchuk, Anthony Szymczyk, and Aleksandr Noy for numerous insightful discussions.

Appendix A. Association constants for multiplets

The procedure used to derive association constants for pairs and triplets can be generalized to larger associates. Note that the volumes V_2, V_3 etc. are obtained by integrating out relevant degrees of freedom, i.e., displacements of ions relative to the lowest-energy ground-state arrangement that increase the energy. For instance, one may move the second ion in Fig. 4A relative to the first ion by translating it along the radial direction x_1, i.e., along the axis connecting the ions. The two other directions x_2 and x_3, orthogonal to x_1, produce rotations of the second ion around the first one. Due to spherical symmetry, rotations do not change the energy U thus they simply contribute a factor $4\pi b^2$ to the phase integral. For small T^*, the monotonic dependence of U on x_1 may be linearized as follows

$$\frac{U}{k_BT} \approx -\frac{\alpha_2}{T^*}(1-\beta_1 x_1), \tag{A1}$$

where $\alpha_{11} = 1$ and $\beta_1 \cong b^{-1}$. The phase integral, Eq. (27), is then approximated for small T^* as follow

$$\int_b^q e^{-U(x_1)/k_BT} 4\pi x_1^2 dx_1 \approx e^{\alpha_2/T^*} 4\pi b^2 \int_0^\infty e^{-\alpha_2\beta_1 x_1/T^*} dx_1 = e^{\alpha_2/T^*} 4\pi b^2 \frac{T^*}{\alpha_{11}\beta_1} \cong 10^1 b^3 T^* e^{\alpha_2/T^*} \tag{A2}$$

A similar factorization may be performed for a third ion added to a pair to form a 2 + 1 triplet (Fig. 4B) The corresponding ground state is the linear arrangement of all three ions. If the principal axis x_1 connects all three ions, the variation of the third ion's energy with x_1 may be linearized similar to Eq. (A1). On the other hand, for rotations in the orthogonal directions x_2 and x_3 (in- and out-plane in Fig. 4B), the energy of the third ions will show a minimum therefore rotations become vibrations and should be approximated, to the leading order, by quadratic terms. $U(x_1, x_2, x_3)$ of the third ion is then approximated as

$$\frac{U}{k_BT} \approx -\frac{\Delta\alpha_3}{T^*}(1-\beta_1 x_1 - \beta_2 x_2^2 - \beta_3 x_3^2), \tag{A3}$$

where, when all three ions are monovalent, $\Delta\alpha_3 = 0.5$, $\beta_1 \cong b^{-1}$ and $\beta_2 = \beta_3 \cong b^{-2}$. Similar to Eq. (A2), after integrating out all degrees of freedom, the linear term $\beta_1 \times_1$ will contribute a factor bT^*, while each quadratic term will contribute approximately a factor (cf. saddle-point integration [102])

$$\int_{-\infty}^{\infty} e^{-\Delta\alpha_3\beta_2 x_2^2/T^*} dx_2 = \left(\frac{\pi T^*}{\beta_2\Delta\alpha_3}\right)^{1/2} \cong bT^{*1/2} \tag{A4}$$

Ultimately, the total factor that multiplies K_2 (Eqs. (28)) to yield K_3 (Eq. (29)) is of the order $b^3T^{*2}e^{\Delta\alpha_3/T^*}$. Again, it may be represented as the product of a ground-state Boltzmann factor $\exp[\Delta\alpha_3/T^*]$ and a residual volume $V_3 \cong 10b^3T^{*2}$, to which the third ion is confined.

It is seen that, for nth ion, starting from the $n = 2$, the ground-state contributes a Boltzmann factor $\exp[\Delta\alpha_n/T^*]$ with $\alpha_n \cong 1$, and each rotational, translational and vibrational degree of freedom contributes to the residual volume V_n a factor of the order b, bT^*, and $bT^{*1/2}$, respectively. In addition, there is a prefactor of the order 10 for each added ion.

This may be illustrated using the general expression for 3 + 1 quadruplets formed by a planar symmetric arrangement of 3 monovalent counter-ions around a central ion of charge z, derived by Aqua et al. The result is [62].

$$K_{31} = Q_{31}\frac{48 2^{1/2} 3^{1/4}\pi^{7/2}}{5\left(z-1/\sqrt{3}\right)^3} b^9 \left(\frac{b}{\lambda_B}\right)^{9/2} \exp\left[\frac{3z-\sqrt{3}}{z\lambda_B/b}\right] \cong 10^3 b^9 T^{*9/2} \exp\left[\frac{\alpha_{31}}{T^*}\right]. \tag{A5}$$

This expression contains a ground-state energy factor $\exp[\frac{\alpha_{31}}{T^*}]$ and the product of three volumes $V_2V_3V_4 \cong 10^3b^9T^{*9/2}$ made up of three rotations (b^3), three symmetric vibrations ($b^3T^{*}3/2$), and three translations (b^3T^{*3}) of the three ions bound to the central ions. When compared to its linear 2 + 1 triplet predecessor (cf. Eq. (28) and Fig. 4B), the volume $V_4 \cong 10b^3T^{*3/2}$may be understood as one contributed by one translation (a factor bT^*) *plus* two vibrations (in-plane and out-of-plane, in total a factor $(bT^{*}1/2)^2 = b^2T^*$, of the fourth ion *minus* the replacement of the in-plane vibration of the third ion with a

rotation (a factor $b/bT^{*1/2} = T^{*}{-}1/2$). The latter is required to change the symmetry, when a linear triplet (Fig. 4B) is transformed to an angular one prior to adding the fourth ion. An expression with somewhat different prefactor and α, but otherwise identical to Eq. (A5) is obtained for symmetric 2 + 2 quadruplets composed of 2 cations and 2 anions in a rhombic ground-state arrangement, confirming the general form.

For still larger multiplets, the parameters $\Delta\alpha_n \sim \alpha_n/n$ and V_n will vary with n, but, apparently, not dramatically. $\Delta\alpha_n$ or ground-state electrostatic energy per ion α_n/n will decrease with n, but fairly slowly. For instance, for equally sized monovalent cations and anions, α_n/n will have the values 0.5, 0.5, 0.391, and 0.280, respectively, for $n = 2$ (pair), 3 (linear triplet), 4 (22 quadruplet), and 8 ($2 \times 2 \times 2$ cubic octet). It is anticipated that for still larger n, ions would tend to arrange in a quasi-crystalline lattice arrangement, for which α_n/n or $\Delta\alpha_n$ would approach an appropriate Madelung constant, while V_n would be determined mainly by the ion vibrations within the quasi-lattice, for which $V_n \cong b^3 T^{*3/2}$. This justifies the use of an approximately constant θ_n in Eq. (30) and Θ in Eqs. (39–41), as a reasonable approximation. Obviously, the conclusion needs to be reconsidered when PM no more applies.

References

[1] Schaefer A, Fane AG, Waite TD. Nanofiltration: Principles and applications. Elsevier; 2005.
[2] Kucera J. Reverse osmosis principles. In: Kucera J, editor. Reverse osmosis: Design, processes, and applications for engineers. Hoboken, NJ, USA: Wiley; 2015 15–9.
[3] Bason S, Freger V. Phenomenological analysis of transport of mono- and divalent ions in nanofiltration. J Membr Sci 2010;360:389–96.
[4] Fridman-Bishop N, Tankus KA, Freger V. Permeation mechanism and interplay between ions in nanofiltration. J Membr Sci 2018;548:449–58.
[5] Grosberg AY, Nguyen TT, Shklovskii BI. The physics of charge inversion in chemical and biological systems. Rev Mod Phys 2002;74:329.
[6] Yaroshchuk A, Bruening ML, Zholkovskiy E. Modelling nanofiltration of electrolyte solutions. Adv Colloid Interface Sci 2019;268:39–63.
[7] Bandini S, Bruni L. Transport phenomena in nanofiltration membranes; 2010.
[8] Marcus Y, Hefter G. Ion pairing. Chem Rev 2006;106:4585–621.
[9] Kgl Bjerrum N. Danske Vid Selskab, Math-fys medd, Vol. 7; 1926; 1–48.
[10] Barthel JM, Krienke H, Kunz W. Physical chemistry of electrolyte solutions: Modern aspects. Springer Science & Business Media; 1998.
[11] Dresner L. Some remarks on the integration of the extended Nernst-Planck equations in the hyperfiltration of multicomponent solutions. Desalination 1972;10:27–46.
[12] Kedem O, Freger V. Determination of concentration-dependent transport coefficients in nanofiltration: defining an optimal set of coefficients. J Membr Sci 2008;310:586–93.
[13] Yaroshchuk AE. Rejection of single salts versus transmembrane volume flow in RO/NF: thermodynamic properties, model of constant coefficients, and its modification. J Membr Sci 2002;198:285–97.
[14] Bason S, Kedem O, Freger V. Determination of concentration-dependent transport coefficients in nanofiltration: experimental evaluation of coefficients. J Membr Sci 2009;326:197–204.
[15] Levich VG. Physicochemical hydrodynamics. New Jersey: Prentice-Hall; 1962.
[16] Spiegler KS, Kedem O. Thermodynamics of hyperfiltration (reverse osmosis): criteria for efficient membranes. Desalination 1966;1:311–26.
[17] Yaroshchuk A, Martínez-Lladó X, Llenas L, Rovira M, de Pablo J. Solution-diffusion-film model for the description of pressure-driven trans-membrane transfer of electrolyte mixtures: one dominant salt and trace ions. J Membr Sci 2011;368:192–201.
[18] Yaroshchuk AE, Ribitsch V. The use of trace ions for advanced characterisation of transport properties of NF membranes in electrolyte solutions: theoretical analysis. J Membr Sci 2002;201:85–94.
[19] Nir O, Bishop NF, Lahav O, Freger V. Modeling pH variation in reverse osmosis. Water Res 2015;87:328–35.
[20] Mazzoni C, Bandini S. On nanofiltration Desal-5 DK performances with calcium chloride–water solutions. Sep Purif Technol 2006;52:232–40.
[21] Bandini S, Mazzoni C. Modelling the amphoteric behaviour of polyamide nanofiltration membranes. Desalination 2005;184:327–36.
[22] Helfferich FG. Ion exchange. Courier Corporation; 1995.
[23] Wang XL, Tsuru T, Nakao S, Kimura S. Electrolyte transport through nanofiltration membranes by the space-charge model and the comparison with Teorell-Meyer-Sievers model. J Membr Sci 1995;103:117–33.
[24] Bowen WR, Mukhtar H. Characterisation and prediction of separation performance of nanofiltration membranes. J Membr Sci 1996;112:263–74.
[25] Levenstein R, Hasson D, Semiat R. Utilization of the Donnan effect for improving electrolyte separation with nanofiltration membranes. J Membr Sci 1996;116:77–92.
[26] Hagmeyer G, Gimbel R. Modelling the salt rejection of nanofiltration membranes for ternary ion mixtures and for single salts at different pH values. Desalination 1998;117:247–56.
[27] Afonso MD, de Pinho MN. Transport of $MgSO_4$, $MgCl_2$, and Na_2SO_4 across an amphoteric nanofiltration membrane. J Membr Sci 2000;179:137–54.
[28] Bowen WR, Welfoot JS. Modelling the performance of membrane nanofiltration – critical assessment and model development. Chem Eng Sci 2002;57:1121–37.
[29] de Pinho MN, Semiao V, Geraldes V. Integrated modeling of transport processes in fluid/nanofiltration membrane systems. J Membr Sci 2002;206:189–200.
[30] Bandini S, Vezzani D. Nanofiltration modeling: the role of dielectric exclusion in membrane characterization. Chem Eng Sci 2003;58:3303–26.
[31] Szymczyk A, Fievet P. Investigating transport properties of nanofiltration membranes by means of a steric, electric and dielectric exclusion model. J Membr Sci 2005;252:77–88.
[32] Lefebvre X, Palmeri J, David P. Nanofiltration theory: an analytic approach for single salts. J Phys Chem B 2004;108:16811–24.
[33] Lefebvre X, Palmeri J. Nanofiltration theory: good co-ion exclusion approximation for single salts. J Phys Chem B 2005;109:5525–40.
[34] Sharma RR, Chellam S. Frictional interpretation of thermodynamic transport parameters for porous nanofiltration membranes. J Water Supply Res Technol Aqua 2006;55:571–87.
[35] Bason S, Kaufman Y, Freger V. Analysis of ion transport in nanofiltration using phenomenological coefficients and structural characteristics. J Phys Chem B 2010;114:3510–7.
[36] Szymczyk A, Fievet P, Bandini S. On the amphoteric behavior of Desal DK nanofiltration membranes at low salt concentrations. J Membr Sci 2010;355:60–8.
[37] Geise GM, Paul DR, Freeman BD. Fundamental water and salt transport properties of polymeric materials. Prog Polym Sci 2014;39:1–42.
[38] Deen W. Hindered transport of large molecules in liquid-filled pores. AIChE J 1987;33:1409–25.
[39] Kosutic K, Kastelan-Kunst L, Kunst B. Porosity of some commercial reverse osmosis and nanofiltration polyamide thin-film composite membranes. J Membr Sci 2000;168:101–8.
[40] Van der Bruggen B, Vandecasteele C. Modelling of the retention of uncharged molecules with nanofiltration. Water Res 2002;36:1360–8.
[41] Dražević E, Košutić K, Kolev V, Freger V. Does hindered transport theory apply to desalination membranes? Environ Sci Technol 2014;48:11471–8.
[42] Koros WJ, Zhang C. Materials for next-generation molecularly selective synthetic membranes. Nat Mater 2017;16:289.
[43] Bereciartua PJ, Cantín Á, Corma A, Jordá JL, Palomino M, Rey F, et al. Control of zeolite framework flexibility and pore topology for separation of ethane and ethylene. Science 2017;358:1068.
[44] Anderson JE, Pusch W. The membrane/water partition coefficients of ions: electrostatic calculations of dielectric heterogeneity. Ber Bunsen Phys Chem 1976;80:846–9.
[45] Yaroshchuk AE. Dielectric exclusion of ions from membranes. Adv Colloid Interface Sci 2000;85:193–230.
[46] Szymczyk A, Fatin-Rouge N, Fievet P, Ramseyer C, Vidonne A. Identification of dielectric effects in nanofiltration of metallic salts. J Membr Sci 2007;287:102–10.
[47] Yaroshchuk AE. Non-steric mechanisms of nanofiltration: superposition of Donnan and dielectric exclusion. Sep Purif Technol 2001;22:143–58.
[48] Robinson RA, Stokes RH. Electrolyte solutions. Dover Pubns; 2002.
[49] Strathmann H. Ion-exchange membrane separation processes. Elsevier; 2004.
[50] Schaep J, Vandecasteele C. Evaluating the charge of nanofiltration membranes. J Membr Sci 2001;188:129–36.
[51] Coronell O, Marinas BJ, Cahill DG. Depth heterogeneity of fully aromatic polyamide active layers in reverse osmosis and nanofiltration membranes. Environ Sci Technol 2011;45:4513–20.
[52] Bason S, Oren Y, Freger V. Characterization of ion transport in thin films using electrochemical impedance spectroscopy II: examination of the polyamide layer of RO membranes. J Membr Sci 2007;302:10–9.
[53] Déon S, Escoda A, Fievet P. A transport model considering charge adsorption inside pores to describe salts rejection by nanofiltration membranes. Chem Eng Sci 2011;66:2823–32.
[54] Efligenir A, Fievet P, Déon S, Salut R. Characterization of the isolated active layer of a NF membrane by electrochemical impedance spectroscopy. J Membr Sci 2015;477:172–82.
[55] Shaffer DL, Feldman KE, Chan EP, Stafford GR, Stafford CM. Characterizing salt permeability in polyamide desalination membranes using electrochemical impedance spectroscopy. J Membr Sci 2019;583:248–57.
[56] Boroudjerdi H, Kim Y-W, Naji A, Netz RR, Schlagberger X, Serr A. Statics and dynamics of strongly charged soft matter. Phys Rep 2005;416:129–99.
[57] Levin Y, Fisher ME. Criticality in the hard-sphere ionic fluid. Phys A Stat Mech Appl 1996;225:164–220.
[58] Hill TL. An introduction to statistical thermodynamics. Courier Corporation; 1986.
[59] Katchalsky A, Alexanrowicz Z, Kedem O. 15 polyelectrolyte solutions. Chemical physics of ionic solutions: A selection of invited papers and discussions, 295. ; 1966.
[60] Manning GS. Limiting laws and counterion condensation in polyelectrolyte solutions I. Colligative properties. J Chem Phys 1969;51:924–33.
[61] Kolev V, Freger V. Molecular dynamics investigation of ion sorption and permeation in desalination membranes. J Phys Chem B 2015;119:14168–79.
[62] Aqua JN, Banerjee S, Fisher ME. Criticality in charge-asymmetric hard-sphere ionic fluids. Phys Rev E 2005;72.
[63] Kamcev J, Paul DR, Manning GS, Freeman BD. Predicting salt permeability coefficients in highly swollen, highly charged ion exchange membranes. ACS Appl Mater Interfaces 2017;9:4044–56.

[64] Kamcev J, Paul DR, Freeman BD. Ion activity coefficients in ion exchange polymers: applicability of Manning's counterion condensation theory. Macromolecules 2015; 48:8011–24.
[65] Parsegian A. Energy of an ion crossing a low dielectric membrane: solutions to four relevant electrostatic problems. Nature 1969;221:844–6.
[66] Zhang XJ, Cahill DG, Coronell O, Marinas BJ. Partitioning of salt ions in FT30 reverse osmosis membranes. Appl Phys Lett 2007;91.
[67] Coronell O, González MI, Mariñas BJ, Cahill DG. Ionization behavior, stoichiometry of association, and accessibility of functional groups in the active layers of reverse osmosis and nanofiltration membranes. Environ Sci Technol 2010;44:6808–14.
[68] Tiraferri A, Elimelech M. Direct quantification of negatively charged functional groups on membrane surfaces. J Membr Sci 2012;389:499–508.
[69] Perry LA, Coronell O. Reliable, bench-top measurements of charge density in the active layers of thin-film composite and nanocomposite membranes using quartz crystal microbalance technology. J Membr Sci 2013;429:23–33.
[70] Lifson S, Jackson JL. On the self-diffusion of ions in a polyelectrolyte solution. J Chem Phys 1962;36:2410–4.
[71] Manning GS. Limiting laws and counterion condensation in polyelectrolyte solutions II. Self-diffusion of the small ions. J Chem Phys 1969;51:934–8.
[72] Zwanzig R. Diffusion in a rough potential. Proc Natl Acad Sci 1988;85:2029–30.
[73] Torquato S. Random heterogeneous materials: Microstructure and macroscopic properties. New York: Springer-Verlag; 2002.
[74] Freger V. Swelling and morphology of the skin layer of polyamide composite membranes: an atomic force microscopy study. Environ Sci Technol 2004;38:3168–75.
[75] Freger V, Ben-David A. Use of attenuated total reflection infrared spectroscopy for analysis of partitioning of solutes between thin films and solution. Anal Chem 2005;77:6019–25.
[76] Ben-David A, Bason S, Jopp J, Oren Y, Freger V. Partitioning of organic solutes between water and polyamide layer of RO and NF membranes: correlation to rejection. J Membr Sci 2006;281:480–90.
[77] Levchenko S, Freger V. Breaking the symmetry: mitigating scaling in tertiary treatment of waste effluents using a positively charged nanofiltration membrane. Environ Sci Technol Lett 2016;3:339–43.
[78] Freger V. Elastic energy in microscopically phase-separated swollen polymer networks. Polymer 2002;43:71–6.
[79] Zhang XJ, Cahill DG, Coronell O, Marinas BJ. Absorption of water in the active layer of reverse osmosis membranes. J Membr Sci 2009;331:143–51.
[80] Lee J, Doherty CM, Hill AJ, Kentish SE. Water vapor sorption and free volume in the aromatic polyamide layer of reverse osmosis membranes. J Membr Sci 2013;425: 217–26.
[81] Kim SH, Kwak SY, Suzuki T. Positron annihilation spectroscopic evidence to demonstrate the flux-enhancement mechanism in morphology-controlled thin-film-composite (TFC) membrane. Environ Sci Technol 2005;39:1764–70.
[82] Coronell O, BJ Mari±as, Zhang X, Cahill DG. Quantification of functional groups and modeling of their ionization behavior in the active layer of FT30 reverse osmosis membrane. Environ Sci Technol 2008;42:5260–6.
[83] Kolev V, Freger V. Hydration, porosity and water dynamics in the polyamide layer of reverse osmosis membranes: a molecular dynamics study. Polymer 2014;55: 1420–6.
[84] Muthukumar M. Theory of counter-ion condensation on flexible polyelectrolytes: adsorption mechanism. J Chem Phys 2004;120:9343–50.
[85] Fridman-Bishop N, Freger V. When salt-rejecting polymers meet protons: an electrochemical impedance spectroscopy investigation. Langmuir 2017;33: 1391–7.
[86] Fridman-Bishop N, Freger V. What makes aromatic polyamide membranes superior: new insights into ion transport and membrane structure. J Membr Sci 2017; 540:120–8.
[87] Yaroshchuk A, Bruening ML. An analytical solution of the solution-diffusion-electromigration equations reproduces trends in ion rejections during nanofiltration of mixed electrolytes. J Membr Sci 2017;523:361–72.
[88] Biesheuvel PM, Zhang L, Gasquet P, Blankert B, Elimelech M, van der Meer WGJ. Ion selectivity in brackish water desalination by reverse osmosis: theory, measurements, and implications. Environ Sci Technol Lett 2020;7:42–7.
[89] Kotelyanskii M, Wagner N, Paulaitis M. Molecular dynamics simulation study of the mechanisms of water diffusion in a hydrated, amorphous polyamide. Comput Theor Polym Sci 1999;9:301–6.
[90] Harder E, Walters DE, Bodnar YD, Faibish RS, Roux B. Molecular dynamics study of a polymeric reverse osmosis membrane. J Phys Chem B 2009;113: 10177–82.
[91] Hughes ZE, Gale JD. A computational investigation of the properties of a reverse osmosis membrane. J Mater Chem 2010;20:7788–99.
[92] Ding M, Szymczyk A, Goujon F, Soldera A, Ghoufi A. Structure and dynamics of water confined in a polyamide reverse-osmosis membrane: a molecular-simulation study. J Membr Sci 2014;458:236–44.
[93] Chang K-S, Huang Y-H, Lee K-R, Tung K-L. Free volume and polymeric structure analyses of aromatic polyamide membranes: a molecular simulation and experimental study. J Membr Sci 2010;354:93–100.
[94] Xiang Y, Liu Y, Mi B, Leng Y. Hydrated polyamide membrane and its interaction with alginate: a molecular dynamics study. Langmuir 2013;29:11600–8.
[95] Shen M, Keten S, Lueptow RM. Dynamics of water and solute transport in polymeric reverse osmosis membranes via molecular dynamics simulations. J Membr Sci 2016;506:95–108.
[96] Song Y, Xu F, Wei M, Wang Y. Water flow inside polamide reverse osmosis membranes: a non-equilibrium molecular dynamics study. J Phys Chem B 2017;121: 1715–22.
[97] Zhang H, Wu MS, Zhou K, AW-K Law. Molecular insights into the composition-structure-property relationships of polyamide thin films for reverse osmosis desalination. Environ Sci Technol 2019;53:6374–82.
[98] Luo Y, Harder E, Faibish RS, Roux B. Computer simulations of water flux and salt permeability of the reverse osmosis FT-30 aromatic polyamide membrane. J Membr Sci 2011;384:1–9.
[99] Ding M, Szymczyk A, Ghoufi A. On the structure and rejection of ions by a polyamide membrane in pressure-driven molecular dynamics simulations. Desalination 2015;368:76–80.
[100] Devanathan R, Idupulapati N, Baer MD, Mundy CJ, Dupuis M. Ab initio molecular dynamics simulation of proton hopping in a model polymer membrane. J Phys Chem B 2013;117:16522–9.
[101] Zelovich T, Vogt-Maranto L, Hickner MA, Paddison SJ, Bae C, Dekel DR, et al. Hydroxide ion diffusion in anion-exchange membranes at low hydration: insights from ab initio molecular dynamics. Chem Mater 2019;31:5778–87.
[102] Arfken GB, Weber HJ. Mathematical methods for physicists. AAPT; 1999.